ISET Journal of Earthquake Technology, Paper No. 515, Vol. 48, No. 1, March 2011, pp. 29–60

INVESTIGATION AND ANALYSIS OF SEISMIC WAVE PARAMETERS OF SEISMIC GAP, SEISMIC BELT AND FORESHOCK

Wenlong Liu*, Yucheng Liu**, Yonglin Xu*, Chun Zhang*, Huan Zhang*, Weidong Shen* and Weixing Zhong*

*Earthquake Administration of Shanghai Municipality
Shanghai 200062, China
**Department of Mechanical Engineering, University of Louisiana
Lafayette, LA 70504, U.S.A.

ABSTRACT

Four earthquakes with magnitudes around M 6.0, which occurred in southeastern China since 1970, are studied based on six seismic wave parameters. These parameters include the rupture characteristic L_0/L, primary rupture directions, the ambient shear stress τ, the temporal periodicity of waveform, r, Q values for P-waves, and the width of Fourier spectrum, w. In this study, the six parameters for each earthquake are calculated, compared, and investigated in order to define single foreshocks. Errors caused by the digitization of analog records and application of simplified hypocenter and medium models, as well as the errors generated in measuring earthquake magnitude and hypocentral radius, are estimated and discussed. Primary characteristics of the earthquakes that occurred within the seismogenic zones and seismic belts are presented after processing 510 charts, 135 earthquakes, and 1030 records.

KEYWORDS: Rupture Characteristics, Ambient Stress, Seismic Gap, Seismic Belt, Foreshock

INTRODUCTION

Since the late 1970s, the earthquake activity method has been fully developed in China and used as the most important method for predicting earthquakes. In this method, earthquakes are predicted based on the seismic gap, seismic belt, and foreshock. A seismic gap is a segment of an active fault that has not slipped in an unusually long time, when compared with the other segments along the same structure. A seismic belt is a narrow geographic zone on the Earth's surface, along which most earthquake activity occurs. A foreshock is a minor earthquake preceding a major earthquake.

The seismic gap hypothesis states that earthquake hazard increases with time since the last large earthquake on certain faults or plate boundaries. The applications of the seismic gap theory to earthquake forecasting were fully demonstrated by Kagan and Jackson (1991, 1995) and Lahr and Plafker (1980). In the earthquake activity method, anomalies in the seismic gap and belt have long been considered as possible precursors of the mid-strong earthquakes. Peacock et al. (1988) observed the temporal variations of shear wave splitting in the Anza seismic gap, Southern California, and used the wave splitting to monitor the detailed changes in the build-up of stress before an earthquake. Davies et al. (1981) expected a great earthquake occurring along the Alaska-Aleutian plate boundary within a reasonable span of time, based on a thorough investigation of the Shumagin seismic gap. Kostoglodov et al. (2003) measured the parameters of the Guerrero seismic gap, and based on the results they initiated a reassessment of the seismic potential of Guerrero and other seismic gaps in Mexico. Seismic gaps and belts have also been used for predicting long-term earthquakes in Gansu, China (Gaudemer et al., 1995) and east of Guadeloupe (Dorel, 1981).

The determination of the seismic gap and belt has suffered from subjective arbitrariness, which leads to errors and omissions in the earthquake prediction. Also, the single foreshock of the main shock cannot be identified out of the earthquake sequences, which have occurred before the main shock, by using the seismic activity method (the single foreshock is a conventional term used in seismology). It is known that the abnormal phenomena of the seismic gap, belt and foreshock are the results of the variations of stress conditions and medium characteristics in the hypocenter area. The information on these variations must be carried by the seismic wave. Therefore, by identifying and extracting the information from the seismic wave, an earthquake can be predicted more accurately and its physical mechanism can also be described.

EARTHQUAKE SAMPLES

Since 1970s there have been four earthquakes with magnitudes around 6.0 in southeastern China, which were recorded clearly and completely. Those earthquakes are (a) M 6.0 earthquake near Liyang, Jiangsu province on July 9, 1979, (b) M 5.9 earthquake near Heze, Shandong province on November 7, 1983, (c) M 6.2 earthquake in southern Yellow Sea on May 21, 1984, and (d) M 6.1 and M 6.2 earthquakes in northern Gulf on December 31, 1994 and January 10, 1995, respectively (see Figure 1).

Fig. 1 Distribution of earthquake samples

For each of the above earthquakes, the anomalous seismicity pattern of the earthquake is studied as well as the space-time-range of the earthquake, based on the data given in Zhang et al. (1990a, 1990b) and Chen et al. (2002). In order to investigate the radiation of seismic waves during foreshocks, two foreshocks are selected: (a) the magnitude 4.6 earthquake that occurred in Lishui, Jiangsu province on May 10, 1977 (i.e., the foreshock of the Liyang earthquake), and (b) the magnitude 4.8 earthquake that occurred in Ci County, Hebei province on May 29, 1982 (i.e., the foreshock of the Heze earthquake). It needs to be mentioned that there is no universal quantitative criterion for distinguishing what is anomalous from what is normal, because different regions have different geological features and assume different normal seismicity patterns. Therefore, we have been continuously monitoring the seismic parameters over those areas and taking the values during seismically quiet periods as their normal values. Once we find that one or more parameter values distinctly deviate from their normal values, we consider those as “anomalies” and start to investigate whether those “anomalies” were associated with a potential earthquake.

In selecting the appropriate seismic records and seismograms, we have chosen for digitization the analog data recorded by those seismic observatories, whose epicentral distances were greater than 100 km. The selected data are clear and complete, and vary in appropriate ranges, which is suitable for further analysis. Also, for each of the above earthquakes, in order to determine the rupture characteristics of the earthquake, related seismic records have been read from at least three seismic observatories. Those observatories evenly surround the epicenter, and the field angle of the two farthest observatories and the epicenter is greater than 60^{o}.

1. Applied Methods

1.1 Rupture Characteristics of Medium and Small Earthquakes

Earthquake's rupture characteristics include unilateral rupture or bilateral rupture, and primary rupture direction for the unilateral rupture. Liu et al. (1996) presented a method of using directional function to determine the earthquake's rupture characteristics. This method is described as follows.

We consider an asymmetric bilateral rupture (see Figure 2), whose rupture propagation velocity is v_f, the rupture lengths of the two sides are L_0 and L_π, focal depth h is 0, and the epicentral distance of the seismic observatory is r. The P-wave spectrum of far-field radiation at the seismic observatory is

$$U_r(\omega) = \frac{m_0}{4\pi\rho v_p^3 r} R_\alpha i\omega G(\omega) e^{\frac{i\omega r}{v_p}} \left(\frac{L_0}{L} e^{-ix_0} \frac{\sin x_0}{x_0} + \frac{L_\pi}{L} e^{-ix_\pi} \frac{\sin x_\pi}{x_\pi} \right) \tag{1}$$

where m_0 is the seismic moment, v_p is the P-wave velocity, R_α is the radiation pattern factor, and

$$x_0 = \frac{\omega L_0}{2} \left(\frac{1}{v_f} - \frac{\cos\theta}{v_p} \right) \tag{2a}$$

$$x_\pi = \frac{\omega L_\pi}{2} \left(\frac{1}{v_f} + \frac{\cos\theta}{v_p} \right) \tag{2b}$$

$$R_\alpha = \sin 2\theta \tag{2c}$$

$$L = L_0 + L_\pi \tag{2d}$$

Let the earthquake be recorded by the seismic observatories 1 and 2, and let the epicentral distances of the two observatories be equal to each other (as shown in Figure 2). We assume that the seismogenic fault is a vertical strike-slip fault whose depth is zero, and that both stations are located in the YZ-plane. It is also assumed that the stations 1 and 2 are located on the two lines emanating from the hypocenter along the reverse directions (therefore, the angles between the two stations are θ and $\theta+\pi$, respectively). Then, the ratio between the amplitude spectra obtained from the two observatories can be defined by using a directional function D expressed as

$$D = \left| \frac{U_1(\omega)}{U_2(\omega)} \right| = \left| \frac{e^{-ix_{10}} \sin x_{10} \left(\frac{1}{v_f} + \frac{\cos\theta}{v_p} \right) + e^{-ix_{1\pi}} \sin x_{1\pi} \left(\frac{1}{v_f} - \frac{\cos\theta}{v_p} \right)}{e^{-ix_{20}} \sin x_{20} \left(\frac{1}{v_f} + \frac{\cos\theta}{v_p} \right) + e^{-ix_{2\pi}} \sin x_{2\pi} \left(\frac{1}{v_f} - \frac{\cos\theta}{v_p} \right)} \right| \tag{3}$$

If the field angle between the lines from both observatories to the epicenter is denoted as α ($\neq \pi$), then the ratio between the two amplitude spectra can be defined as a generalized directional function D_G where

$$D_G = \left| \frac{\sin 2\theta \left(\frac{1}{v_f} + \frac{\cos(\theta+\alpha)}{v_p} \right) \left(\frac{1}{v_f} - \frac{\cos(\theta+\alpha)}{v_p} \right)}{\sin 2(\theta+\alpha) \left(\frac{1}{v_f} + \frac{\cos\theta}{v_p} \right) \left(\frac{1}{v_f} - \frac{\cos\theta}{v_p} \right)} \right| \times \left| \frac{e^{-ix_{10}} \sin x_{10} \left(\frac{1}{v_f} + \frac{\cos\theta}{v_p} \right) + e^{-ix_{1\pi}} \sin x_{1\pi} \left(\frac{1}{v_f} - \frac{\cos\theta}{v_p} \right)}{e^{-ix_{20}} \sin x_{20} \left(\frac{1}{v_f} + \frac{\cos(\theta+\alpha)}{v_p} \right) + e^{-ix_{2\pi}} \sin x_{2\pi} \left(\frac{1}{v_f} - \frac{\cos(\theta+\alpha)}{v_p} \right)} \right| \tag{4}$$

From Equation (4), it can be observed that D_G is a function of ω with the parameters α, L_0/L, and θ. As shown in Figure 2 (where the horizontal plane XZ is the fault plane), θ is the azimuth angle between the station 1 and Y-axis (i.e., the vertical direction), and α is the azimuth angle between the observatories 2 and 1. The parameters, L_0/L and θ, can be obtained from field surveying, and once we have those values, a D_G curve can be easily plotted. It needs to be mentioned that in Figure 2, the used coordinate system is not with reference to the geographical coordinates but to the hypocentral coordinates, with the fault plane being a horizontal plane where the rupture propagates along its vertical direction (i.e., the Y-axis). Here, the vertical direction is determined from the hypocentral coordinate system, instead of the geographical coordinate system. The hypocentral coordinate system has been created based on the origin of hypocenter, which is a popular system used in seismology (Giovambattista and Barba, 1997). In determining the primary rupture direction based on the records of two observatories, we first measure the field angle α. Next, we choose six L_0/L values from 0.5 to 1.0 with the increment of 0.1, and 12 values of θ from 0º to 180º with the increment of 15º. Based on these parameters, (6×12 =) 72 generalized directional function curves are calculated from Equation (4). The calculated curves are then compared with the curve recorded by the observatory 1 to find the closest calculated curve and the corresponding values of L_0/L and θ. Two candidates for the primary rupture directions can be obtained by adding/subtracting θ to/from the geographic azimuth of the observatory 1, and one of these must be the true primary rupture direction. If the records of more than three observatories are available, we will be able to obtain more than two generalized directional functions D_G and more than four candidates for the primary rupture directions by following this method. The candidate directions and rupture azimuths are counted based on the four quadrants, and the quadrant where most rupture azimuths are located is selected. The average value of the rupture azimuths in the selected quadrant is then calculated and specified as the primary rupture direction of the earthquake.

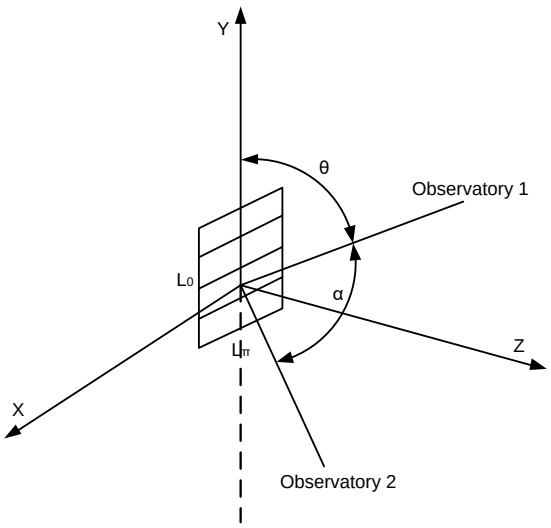

Fig. 2 Asymmetric bilateral rupture (the observatories 1 and 2 are located in the YZ-plane)

1.2 Ambient Shear Stress

The ambient shear stress values can be determined by employing Chen's method (Chen et al., 1977, 1978), because the actual source mechanism of the earthquake samples considered is close to being a horizontal slip. As shown by Chen et al. (1977), the 2-D plane-strain crack mode II can be used to simulate the strike-slip fault and rupture mechanics can be employed to study the earthquake's rupture process to approximate the relationships among the hypocentral parameters and stress conditions as

$$m_s = 2\log(2r_a) + \frac{1}{1.5}\left(\frac{\log 4(1-\nu)\tau^2\eta}{3(2-\nu)\mu} - 11.8\right) \tag{5}$$

$$\frac{D}{2r_a} = \frac{4(1-\nu)\tau^2}{3(2-\nu)\pi\mu\tau_y} \tag{6}$$

$$m_0 = \frac{(1-\nu)\pi\tau^2(2r_a)^3}{3(2-\nu)\tau_y} \tag{7}$$

In these equations r_a is the radius of the rupture circle, ν is the Poisson's ratio (= 0.252 for the crust), μ is the shear modulus (= 33 GPa for the crust), τ denotes the ambient shear stress, η denotes the seismic-wave radiation efficiency (taken as 0.05 in this study), D means the average dislocation, τ_y is the yield strength (taken in this study as 200 MPa for the crust), m_0 is the seismic moment, and m_s denotes the surface wave magnitude. Here, the crack mode II is considered to be the sliding or in-plane shear mode, where the crack surfaces slide over one another in a direction perpendicular to the leading edge of the crack.

By using the dislocation model of circular shear to simulate the medium and small strike-slip earthquakes, taking samples from the seismogram, and then by performing the Fourier analyses, the source spectra can be obtained. From each of these spectra, the spectral amplitude in the lower frequency band, $u(\omega)_{\omega\to 0}$, and the corner frequency $f_{c\alpha}$ can be obtained, and then, the seismic moment m_0 can be determined from

$$u(\omega)_{\omega\to 0} = \frac{m_0}{4\pi\rho v_p^3 r_e} R_\alpha \tag{8}$$

Here, ρ is the density of the medium (taken in this study as 2.7×10^3 kg/m^3 for the crust), r_e is the epicentral distance, the radiation pattern $R_\alpha = \sin 2\theta\cos\varphi$ (if θ and φ are unknown, for small and medium earthquakes we can take the average radiation pattern calculated over the focal sphere), which becomes 4/15 for the P-wave (Venkataraman, 2002), and v_p means the P-wave velocity (taken in this study as 5.7 km/s within the crust; Lidaka et al., 2009). The radius of rupture circle, r_a, can be calculated from the corner frequency $f_{c\alpha}$ since

$$f_{c\alpha} = \frac{0.60}{\left[r_a\left(\frac{1}{v_f} + \frac{\pi}{4v_p}\right)\right]} \tag{9}$$

In Equation (9) the rupture propagation velocity v_f is equal to $0.775v_s$, where v_s is the S-wave velocity (taken in this study as 3.38 km/s within the crust; Wu et al., 1997). Finally, the ambient shear stress τ can be calculated by using the obtained values of m_0 and r_a in Equation (7). Here, we consider the earthquakes with M < 3.0 as "small" earthquakes and the earthquakes with 3.0 < M < 6.0 as "medium" earthquakes.

1.3 Temporal Periodicity of Waveform

A method for determining the temporal periodicity waveform, r, has been proposed by Feng and Yu (1994). According to this method, a certain number of time instants, t_1, t_2, …, t_n, at which the amplitude of displacement or velocity reaches its peak, trough, or zero value, are recorded since the first arrival of P- or S-wave and until one or two wave groups end. The time t_i and the sequence number i are linearly related as

$$t_i = a + b_i \tag{10}$$

where

$$a = \frac{\sum it_i \sum i - \sum t_i \sum i}{\left(\sum i\right)^2 - n\sum i^2} \tag{11}$$

$$b = \frac{n\sum it_i - \sum t_i \sum i\left(i - \dfrac{\sum i}{n}\right)}{\left(\sum i\right)^2 - n\sum i^2} \tag{12}$$

The errors in these estimates of a and b are expressed in terms of their standard deviations estimated as

$$\sigma_a = \sigma_b \frac{\sqrt{\sum i^2}}{n} \tag{13}$$

$$\sigma_b = \frac{(n-1)\sqrt{\sum\left(t_i - \dfrac{\sum t_i}{n}\right)^2}}{n(n-2)\sum\left(i - \dfrac{\sum t_i}{n}\right)^2} \tag{14}$$

The temporal periodicity of waveform, r, is then calculated by using the least squares method as

$$r = \frac{\sum\left[\left(t_i - \dfrac{\sum t_i}{n}\right)\left(i - \dfrac{\sum i}{n}\right)\right]}{\sqrt{\sum\left(t_i - \dfrac{\sum t_i}{n}\right)^2 \sum\left(i - \dfrac{\sum i}{n}\right)^2}} \tag{15}$$

More the waveform deviates from the periodic function, more complicated the rupture process is and higher is the unevenness of the medium and stress distributions at the hypocenter, thus leading to a smaller r. This implies that r is a measure of the complexity of the medium and stress field.

1.3.1 Q Values for P Waves

We assume that a seismic observatory has recorded n earthquakes in one area and that the wave spectrum of the i th earthquake is given by

$$Ai(\varpi) = Ai_0(\varpi)G(Ri)I(\varpi)e^{-\frac{\varpi Ri}{2v_pQ}} \tag{16}$$

where $Ai_0(\varpi)$ is the seismic wave spectrum for the hypocenter, $G(Ri)$ represents the geometric spreading, Ri is the hypocentral distance, $I(\varpi)$ is the instrumental frequency characteristic, $e^{-\frac{\varpi Ri}{2v_pQ}}$ represents the absorption by the medium, and v_p is the P-wave velocity. In order to determine the Q value, two frequencies ω_1 and ω_2 are substituted into Equation (16) to find the frequency ratio:

$$\ln\left|\frac{Ai(\varpi_1)}{Ai(\varpi_2)}\right| = \ln\left|\frac{Ai_0(\varpi_1)}{Ai_0(\varpi_2)}\right| - \frac{(\varpi_1 - \varpi_2)Ri}{2v_pQ} \tag{17}$$

In this equation $(\varpi_1 - \varpi_2)Ri/(2v_pQ)$ is a constant and the $\ln\left|Ai_0(\varpi_1)/Ai_0(\varpi_2)\right|$ value of different recorded earthquakes can also be treated as a constant, if these earthquakes have occurred in the same area and if their magnitudes are close to each other. Thus, the Q values can be directly calculated from Equation (17), which accounts for the features of a different medium before and after the earthquakes.

1.3.2 Width of Fourier Spectrum

The width of Fourier spectrum is defined as the bandwidth. This represents the complexity of seismic waves and is computed for 70% of the maximum spectral amplitude. A wider Fourier spectrum indicates that the seismic waves have more frequency components; therefore, the rupture process should be more complicated and the medium and stress distribution should be more uneven at the hypocenter.

1.4 Data Processing

In this study, the clearly-recorded seismograms with appropriate amplitudes are scanned and digitized through the seismogram digitization and database management system (SDDMS) (Liu et al., 2001). Next, the ranges of the corner frequency $f_{c\alpha}$ for different earthquakes are estimated by using empirical methods, and the window length T is set as 8–10 times the reciprocal of the minimum corner frequency (i.e., $1/(f_{c\alpha})_{\min}$) to improve the resolution of the frequency spectrum. The sampling step size Δt is set as less than $1/(f_{c\alpha})_{\max}$ to avoid the high-frequency aliasing and the resolution is kept as 300 dpi. The digitized records are then connected by lines and re-sampled for an equal time interval. Afterwards, a Hanning window and fast Fourier transform (FFT) are applied to process these records, and the spectra of seismic waves is then obtained after the instrument and medium calibrations. The Hanning window $W(t)$ is taken as

$$W(t)=\begin{cases}\dfrac{1}{2T}\left(1+\cos\dfrac{\pi t}{T}\right) & 0\le t\le T\\ 0 & t<0\end{cases} \tag{18}$$

The theoretical frequency characteristic curves of the instruments corresponding to the seismograms are used for the instrument calibration and the characteristic of the medium frequency, $B(\omega)$, is expressed as

$$B(\omega)=2\exp\left(-\frac{|\omega|r}{2v_pQ}+i\frac{\omega r}{2\pi v_pQ}\ln\left|\left(\frac{\omega}{\omega_0}\right)^2-1\right|\right) \tag{19}$$

where the low cutoff frequency ω is taken as 0.25 Hz and the quality factor Q is taken as 400. Finally, the rupture characteristics of small earthquakes and the ambient shear stress are determined by the methods illustrated above. The Q values of P-waves are estimated directly from the recorded wave spectrum by applying the methods presented above. The time instants of the peaks and troughs in P- or S-waves are measured from the SDDMS (Liu et al., 2001) and the temporal periodicity waveform is then determined by using Equation (15). Similarly, the width of Fourier spectrum is also obtained from the SDDMS.

2. Analysis of Liyang M 6.0 Earthquake

2.1 Analysis of Rupture Characteristics

Table 1 lists the calculated results of the rupture characteristics of medium and small earthquakes that have occurred before and after the Liyang M 6.0 earthquake. In our study, the earthquakes that have occurred within three years before the main shock are selected to represent the "abnormal" earthquakes that occur during the earthquake preparation process in a seismogenic zone. Further, those earthquakes that have occurred over a long time after the main shock (13 years in the case of Liyang earthquake) are selected to represent the "normal" earthquakes for comparison. It is assumed that this time lag allows the seismogenic zone to return to its normal status after a mid-strong earthquake.

It may be observed in Table 1 that the parameter L_0/L varies from 0.5 to 1.0. Further, it may be mentioned that λ s and σ s denote the azimuths of primary rupture directions and their root-mean-square errors (RMSEs), respectively (λ and σ values are not used, if three or more possible primary rupture directions have been found), and that n is the number of seismic observatories. The certainty factor (CF) of the primary rupture direction is defined as CF = I when $\sigma \le 15°$ and only one primary rupture direction

has been determined, CF = II when $15° < \sigma \leq 30°$ and only one primary rupture direction has been determined, and CF = III when two possible primary directions have been found.

Table 1: Rupture Characteristics of Medium and Small Earthquakes That Occurred before and after Liyang M 6.0 Earthquake

No.	Date	Time	Longitude	Latitude	M_L	L_0/L	λ_1, σ_1 (°)	λ_2, σ_2 (°)	n	CF
Before Liyang M 6.0 earthquake										
1	1977-05-10	11:56	119°13’	31°58’	4.6	0.95			5	
2	1977-09-10	21:35	117°56’	32°59’	2.8	1.0	331.4, 22.5		3	II
3	1977-11-08	21:05	117°30’	32°00’	2.6	0.87	317, 8.7		4	I
4	1977-11-28	05:22	116°53’	32°45’	2.1	1.0			2	
5	1978-01-28	13:01	117°32’	32°11’	2.8	1.0	205.3, 12.1		3	I
6	1978-01-28	13:48	117°37’	32°11’	3.1	0.88	290.8, 7.2	28.3, 7.2	5	III
7	1978-02-16	08:42	117°32’	31°59’	2.8	1.0			2	
8	1978-03-26	04:03	117°31’	32°02’	3.3	0.9	302.1, 9.4		6	I
9	1978-03-26	20:51	118°43’	33°15’	3.6	0.88	309.1, 17.7		7	II
10	1978-04-14	04:40	117°21’	32°29’	3.0	1.0			2	
11	1978-05-28	14:13	117°32’	32°02’	3.2	0.93	186.6, 5	116.6, 5	5	III
12	1978-06-25	04:34	119°17’	31°27’	3.0	1.0			2	
13	1978-07-06	11:44	120°57’	32°43’	3.7	0.93	303.4, 17.3		5	II
14	1978-07-17	00:48	120°50’	32°45’	3.9	0.78	306.7, 19.7		5	II
15	1978-07-17	00:52	120°59’	32°46’	3.3	0.73	42.7, 13.7		4	I
16	1978-07-27	20:30	117°27’	31°57’	3.1	0.90	247.4, 15	352.4, 0	4	III
17	1978-11-24	23:38	117°27’	32°22’	3.3	0.70	212.7, 25		4	II
18	1978-12-01	01:03	119°37’	31°43’	3.3	1.0	301, 30		3	II
19	1978-12-19	08:07	119°00’	32°22’	2.8	1.0			2	
20	1978-12-23	10:53	117°36’	32°10’	3.3	1.0	214.2, 17.3		4	II
21	1979-01-25	18:25	120°12’	33°20’	3.1	0.93	20.6, 7.5		4	I
22	1979-04-16	05:27	117°04’	32°57’	2.2	1.0			2	
23	1979-04-28	09:15	121°27’	32°53’	3.0	1.0			2	
After Liyang M 6.0 earthquake										
24	1992-01-25	06:37	119°51’	31°55’	3.2	0.76	45.7, 0		6	I
25	1992-03-20	23:10	120°04’	32°08’	2.8	0.90	199.7, 7.2	327.2, 7.2	5	III
26	1992-05-29	16:33	120°38’	33°29’	3.3	1.0			2	
27	1992-06-27	07:35	117°46’	32°30’	3.0	1.0	243.3, 15	153.3, 15	4	III
28	1992-09-13	03:47	117°07’	32°08’	2.5	0.90	191.4, 0		3	I
29	1992-10-25	17:46	120°34’	32°45’	3.5	1.0	135.5, 12		8	I

As shown in Table 1, there are 23 earthquakes that have occurred before the Liyang M 6.0 earthquake. Eleven of these (i.e., ≈ 47.8%) had the L_0/L values of 1.0, six earthquakes (i.e., ≈ 26.1%) had the L_0/L values between 0.90 and 0.99, three earthquakes (i.e., ≈ 13.0%) had the L_0/L values between 0.80 and 0.89, and the remaining three earthquakes (≈ 13.0%) had the L_0/L values between

0.70 and 0.79. The average L_0/L value of the 23 earthquakes is 0.93. Among the six earthquakes that occurred after the Liyang earthquake, there were three earthquakes (i.e., 50%) that had the L_0/L values of 1.0, two earthquakes (i.e., ≈ 33.3%) had the L_0/L values between 0.90 and 0.99, and one earthquake (i.e., ≈ 16.7%) had the L_0/L value between 0.70 and 0.79. The average L_0/L value of these six earthquakes is also 0.93. Thus, there has been no obvious change in the average L_0/L value from that before the Liyang earthquake to that after the earthquake.

In Table 1, the M 4.6 earthquake occurred on May 10, 1977, i.e., two years before the Liyang earthquake, and had the L_0/L value of 0.95, which is very close to that for the unilateral rupture. The epicentral distance of this earthquake was 60 km. Until the occurrence of the Liyang earthquake, no earthquake with magnitude higher than M 4.6 occurred in this area; therefore, the M 4.6 earthquake can be considered as the foreshock of the Liyang earthquake.

Figure 3 shows the primary rupture directions of the small and medium earthquakes on the seismogenic zone that occurred before the Liyang earthquake. Figure 4 displays the primary rupture directions of the other small and medium earthquakes that occurred in the same area. From Figure 3 it can be seen that the primary rupture directions of the earthquakes that occurred before the main shock are concentrated on several directions but most of those are pointing out from the gap. Figure 3 has been drawn manually and it only aims at showing all the directions pointing outwards. It may be seen from Table 1 that these directions are roughly parallel to the nodal planes of the main shock (Chen et al., 1997). However, as shown in Figure 4, the primary rupture directions of the earthquakes that occurred during the normal periods (i.e., the periods during which no earthquakes occurred and no anomalies were observed) are disorganized.

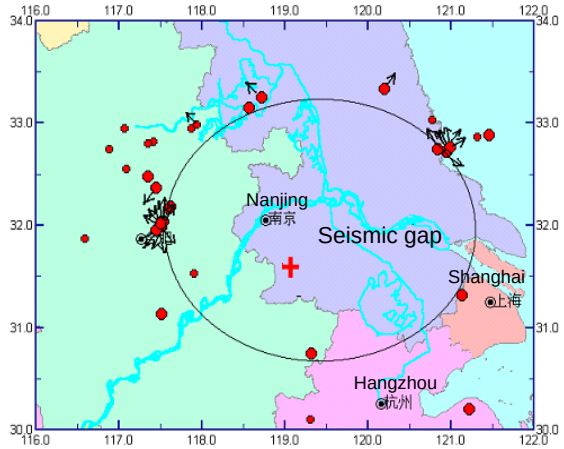

Fig. 3 Primary rupture directions of small and medium earthquakes on the seismogenic zone of the Liyang M 6.0 earthquake

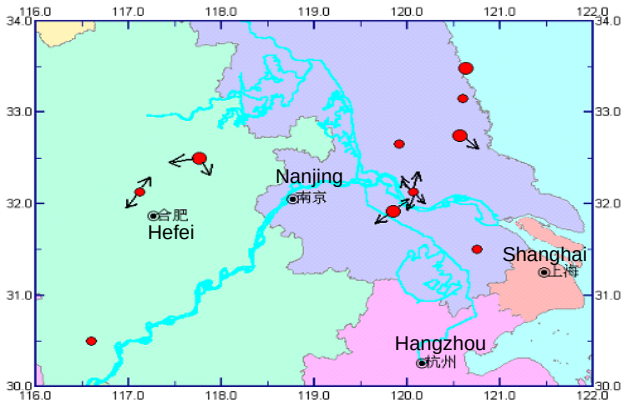

Fig. 4 Primary rupture directions of small and medium earthquakes that occurred during the normal periods in Liyang area

2.2 Calculation of Ambient Shear Stress, Temporal Periodicity of Waveform, Q Value and Width of Fourier Spectrum

The ambient shear stress τ, the temporal periodicity of waveform, r, Q value, and the width of Fourier spectrum, w, of small and medium earthquakes that occurred during the Liyang M 6.0 earthquake sequence are calculated and listed in Table 2. In this table, Q_1 refers to the Q values recorded on those locations where the epicentral distance was less than 130 km, and these values reflect the quality factors of a shallow medium. Q_2 refers to the Q values recorded on those locations where the epicentral distance was between 130 and 300 km, and these values represent the quality factors of a deep medium.

Table 2: τ, r, Q, w of Small and Medium Earthquakes That Occurred during Liyang M 6.0 Earthquake Sequence

No.	Date	Time	Longitude	Latitude	M_L	τ (bar)	r ($\times 10^{-1}$)	Q_1	Q_2	w (Hz)
Before Liyang M 6.0 earthquake										
1	1977-05-10	11:56	119°13’	31°58’	4.6	90.3	9.97		283	0.26
2	1977-09-10	21:34	117°52’	32°57’	2.4	2.5	9.94	106		0.10
3	1977-09-10	21:35	117°56’	32°59’	2.8	10.4	9.94	127		0.10
4	1977-09-13	6:44	117°54’	31°32’	2.1	1.7	9.97	35		0.11
5	1977-09-19	15:33	119°18’	30°06’	2.0	2.0	9.97	290		0.25
6	1977-11-05	02:38	121°13’	30°12’	3.6	6.7	9.93		299	0.66
7	1977-11-08	21:05	117°30’	32°00’	2.6	1.4	9.94	158	562	0.27
8	1977-11-26	17:39	119°10’	31°21’	2.0	0.9	9.87	153		0.25
9	1977-11-28	05:22	116°53’	32°45’	2.1	1.2	9.84	157		0.11
10	1978-01-05	18:41	121°08’	31°19’	3.0	7.0	9.98		158	0.10
11	1978-01-28	13:01	117°32’	32°11’	2.8	8.2	9.74		260	0.15
12	1978-01-28	13:48	117°37’	32°11’	3.1	8.7	9.99	206	176	0.18
13	1978-02-12	05:30	118°34’	33°09’	3.4	6.8	9.96		351	0.22
14	1978-02-16	08:42	117°32’	31°59’	2.8	9.7	9.94	77	242	0.45
15	1978-03-26	04:03	117°31’	32°02’	3.3	8.4	9.96	46	275	0.20
16	1978-03-26	20:51	118°43’	33°15’	3.6	8.3	9.84		576	0.21
17	1978-04-14	04:40	117°21’	32°29’	3.0	10.4	9.99		260	0.42
18	1978-05-28	14:13	117°32’	32°02’	3.2	8.2	9.95		381	0.27
19	1978-06-25	04:34	119°17’	31°27’	3.0	8.4	9.97		353	0.22
20	1978-07-06	11:44	120°57’	32°43’	3.7	37.7	9.97		408	0.23
21	1978-07-06	12:23	120°55’	32°44’	2.8	11.4	9.90		353	0.10
22	1978-07-17	00:48	120°50’	32°45’	3.9	44.0	9.91		472	0.20
23	1978-07-17	00:52	120°59’	32°46’	3.3	11.0	9.96		371	0.60
24	1978-07-17	14:19	120°46’	33°02’	2.6	9.0	9.89		371	0.60
25	1978-07-22	20:45	120°57’	32°42’	2.7	1.3	9.86		175	0.36
26	1978-07-27	20:30	117°27’	31°57’	3.1	9.1	9.81	161	276	0.35
27	1978-08-07	04:51	121°19’	32°53’	2.6	1.9	9.54		188	0.10
28	1978-08-27	22:32	119°22’	31°36’	2.1	1.9	9.83	57		0.42
29	1978-10-02	04:04	120°31’	32°03’	2.7	1.6	9.95		282	0.16
30	1978-10-21	11:19	117°31’	31°08’	3.1	9.3	9.89		261	0.10
31	1978-11-05	13:12	117°05’	32°33’	2.7	2.0	9.99		253	0.32
32	1978-11-17	22:31	119°44’	31°41’	2.7	2.1	9.98		229	0.16
33	1978-11-18	07:52	119°40’	31°43’	2.7	1.1	9.70		203	0.14
34	1978-11-24	23:38	117°27’	32°22’	3.3	12.4	9.98	317	478	1.10
35	1978-12-01	01:03	119°37’	31°43’	3.3	10.8	9.96		450	0.11
36	1978-12-19	08:07	119°00’	32°22’	2.8	16.4	9.97	279	469	0.41
37	1978-12-23	10:53	117°36’	32°10’	3.3	13.7	9.98	194	257	0.38
38	1979-01-02	18:11	116°35’	31°52’	2.2	9.0	9.34			0.25

39	1979-01-25	18:25	120°12’	33°20’	3.1	10.4	9.97		333	0.25
40	1979-02-17	02:42	117°25’	32°49’	2.1	9.0	9.61			0.25
41	1979-02-17	05:53	117°21’	32°48’	2.1	1.3	9.66			0.88
42	1979-03-07	05:08	119°19’	30°45’	3.9	54.6	9.88			0.10
43	1979-04-16	05:27	117°04’	32°57’	2.2	3.1	9.88	219		0.28
44	1979-04-28	09:15	121°27’	32°53’	3.0	8.7	9.96		230	0.39
45	1979-07-08	21:25	117°30’	32°01’	3.2	11.4	9.98		380	0.38
After Liyang M 6.0 earthquake										
46	1992-01-25	06:37	119°51’	31°55’	3.2	9.3	9.96		423	0.21
47	1992-03-20	23:10	120°04’	32°08’	2.8	10.5	9.98		364	0.15
48	1992-05-29	16:33	120°38’	33°29’	3.3	9.7	9.99		417	0.14
49	1992-06-27	07:35	117°46’	32°30’	3.0	3.4	9.97		349	0.64
50	1992-09-13	03:47	117°07’	32°08’	2.5	2.1	9.94	161	265	0.38
51	1992-09-15	10:10	120°45’	31°30’	2.9	12.7	9.94		493	0.32
52	1992-09-23	09:37	116°36’	30°30’	2.6	1.4	9.97		304	1.18
53	1992-10-13	17:59	120°06’	33°09’	2.6	1.3	9.97		203	0.16
54	1992-10-25	17:46	120°34’	32°45’	3.5	10.1	9.96		383	0.16

Figure 5 shows the variation of the ambient shear stress during the Liyang earthquake sequence. From Table 2 and Figure 5, it may be observed that before the Liyang M 6.0 earthquake, the maximum shear stress was higher and that the ambient shear stress varied more violently. However, after the earthquake, the shear stress value stayed at a lower level and varied smoothly.

The variation of the temporal periodicity of waveform, r, is displayed in Figure 6. From this figure and Table 2, it may be seen that the temporal periodicity changed violently during the year preceding the Liyang M 6.0 earthquake (i.e., from August 7, 1978 to July 8, 1979) and that the minimum value of r is 0.934. However, during other periods, the temporal periodicity varied in the range 0.99±0.1.

The variations of Q values and the width of Fourier spectrum, w, are plotted in Figures 7–9. From these figures, it may be inferred that there were no obvious differences in the variations of Q and w before and after the Liyang earthquake. Further, as shown in Table 2, the Q_2 values are generally greater than the Q_1 values. This suggests that the quality factors of a deep medium are higher than those of a shallow medium.

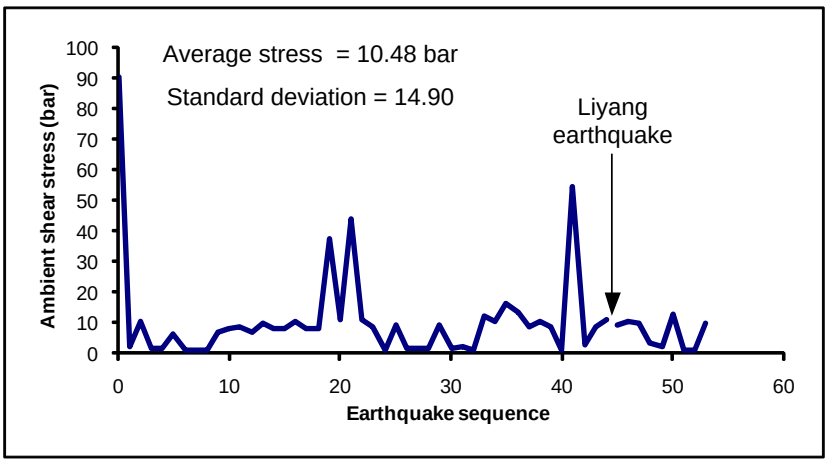

Fig. 5 Ambient shear stress τ of small and medium earthquakes in the Liyang M 6.0 earthquake sequence

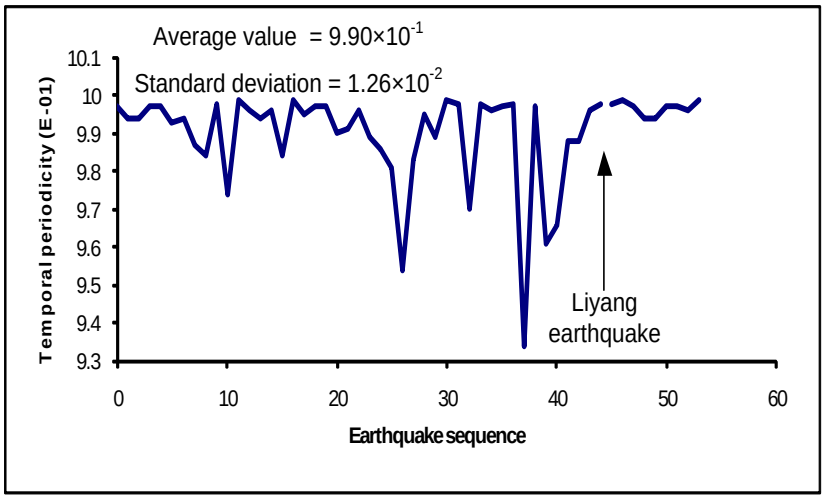

Fig. 6 Temporal periodicity of waveform, r, of small and medium earthquakes in the Liyang M 6.0 earthquake sequence

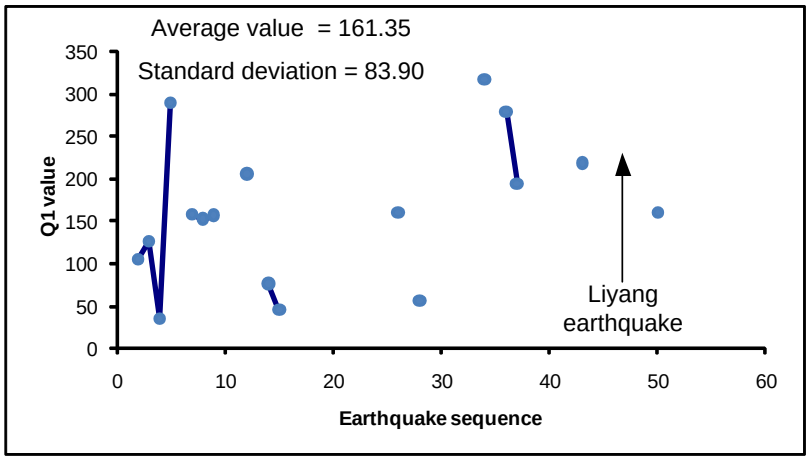

Fig. 7 Q_1 values of the P-waves of small and medium earthquakes in the Liyang M 6.0 earthquake sequence

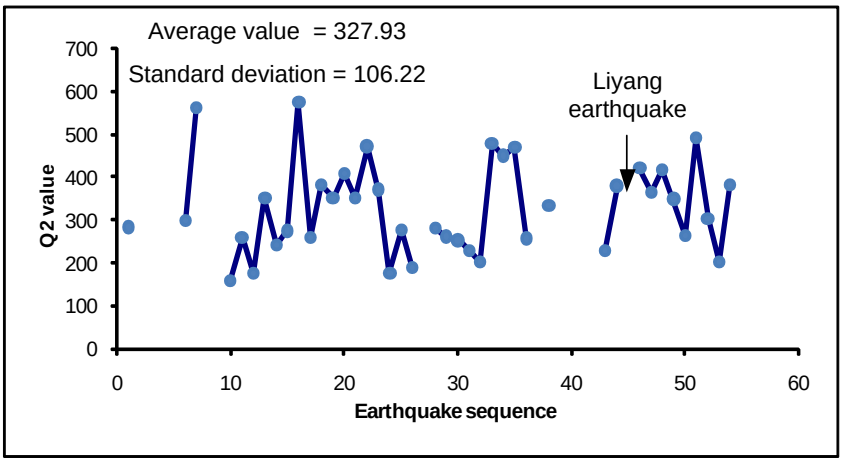

Fig. 8 Q_2 values of the P-waves of small and medium earthquakes in the Liyang M 6.0 earthquake sequence

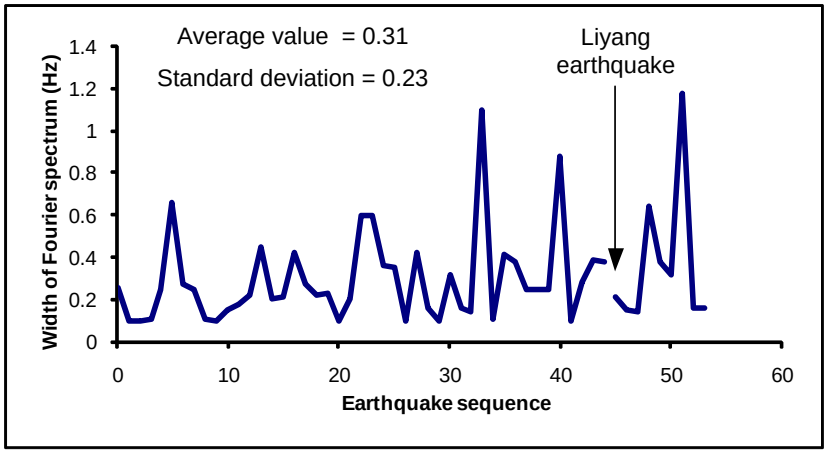

Fig. 9 Fourier spectral width w of small and medium earthquakes in the Liyang M 6.0 earthquake sequence

2.3 Discussion on Liyang M 6.0 Earthquake

Based on the above analyses, the following conclusions are drawn for the Liyang earthquake sequence:

1. The primary rupture directions of the earthquakes that occurred on the seismogenic zone were parallel to the nodal plane of the following main shock. Further, they were either tangent to the zone or pointed towards outside the zone. During the normal periods, the primary rupture directions were disorganized.
2. A few of the high ambient shear stress values and turbulent variations in the shear stress were observed over the year preceding the main shock, and in other times these values were lower and varied smoothly. As shown in Table 2, during the year preceding the Liyang earthquake, the mean stress value was 11.23 bar with the standard deviation of 16.13 bar, while after this earthquake, the mean stress value dropped to 6.72 bar and the standard deviation became 4.84 bar. The median stress value during the year preceding the Liyang earthquake was 9.05 bar and this value was reduced to 8.25 bar during other times.
3. The temporal periodicity of waveform, r, changed violently and several lower values appeared during the year preceding the main shock. The minimum value of r was 0.934. During the normal periods, r varied in the range 0.99 ± 0.01.
4. The M 4.6 earthquake occurred two years before the Liyang earthquake and its epicentral distance was 60 km. Until the occurrence of the main shock, no earthquake with magnitude higher than M 4.6 had occurred in this area. This earthquake was close to the unilateral rupture and its ambient shear stress value was much higher than that for the other earthquakes; therefore, this earthquake could be considered as the foreshock of the Liyang earthquake. Also, as shown in Figure 5, the ambient shear stress τ (= 90.3 bar) for the foreshock was much higher than the stress values for the other earthquakes.
5. No distinct regularity has been found for the variations in the rupture characteristic L_0/L, Q values for P-waves and width of Fourier spectrum before and after the Liyang M 6.0 earthquake.

3. Analysis of Heze M 5.9 Earthquake

3.1 Analysis of Rupture Characteristics

The rupture characteristics of the medium and small earthquakes that occurred before and after the Heze M 5.9 earthquake are listed in Table 3. From this table, the median L_0/L value for the four earthquakes preceding the Heze M 5.9 earthquake is calculated to be 0.91, and the average L_0/L value for the six earthquakes occurring after the Heze earthquake is obtained as 0.89. There is no obvious variation in the L_0/L value in the earthquakes before and after the Heze earthquake. It is also noticed that there are two earthquakes (M_L 4.6 earthquake on January 17, 1982, and M_L 4.8 earthquake on

May 29, 1982) with the L_0/L values of 1.0, which corresponds to the unilateral rupture, and with their occurrences before the Heze earthquake.

Table 3: Rupture Characteristics of Medium and Small Earthquakes That Occurred before and after Heze M 5.9 Earthquake

No.	Date	Time	Longitude	Latitude	M_L	L_0/L	λ_1,σ_1 (°)	λ_2,σ_2 (°)	n	CF
Before Heze M 5.9 earthquake										
1	1981-12-23	06:27	115°26’	35°36’	4.6	1.0	287, 10		3	I
2	1982-01-17	14:57	115°00’	35°04’	3.1	0.75	342.1, 0	352.1, 0	3	III
3	1982-05-29	18:28	114°57’	36°58’	4.8	1.0	200.4, 7.5	65.4, 7.5	3	III
4	1982-07-28	01:23	115°09’	35°00’	4.0	0.90	232.2, 11.3	284.7, 11.3	6	III
After Heze M 5.9 earthquake										
5	1990-02-20	19:49	115°14’	35°14’	3.0	0.90	324.4, 11.0		9	I
6	1990-07-12	07:39	115°22’	35°20’	3.0	0.93	222.7, 14.7		5	I
7	1991-11-11	03:09	115°06’	35°01’	3.2	0.95	246.1, 4.6	311.1, 4.6	9	III
8	1993-12-03	03:49	115°25’	35°21’	3.0	0.90	236.8, 9.8		8	I
9	1994-08-28	22:04	115°26’	35°16’	2.6	0.77	208.4, 7.5	313.4, 7.5	4	III
10	1995-04-14	10:56	115°44’	35°51’	2.7	0.90	189.1, 5	289.1, 5	4	III

Figure 11 shows the primary rupture directions of the small and medium earthquakes that occurred on the seismic belt before the Heze earthquake. Only three samples are available for these earthquakes and two of those had two possible primary rupture directions in each case. In Figure 11 it is observed that one of the possible primary rupture directions of the two samples is consistent with the primary rupture direction of the third sample, which is assumed as the primary rupture direction. Thus, the primary rupture directions of the earthquakes on the seismic belt are conjugated to the direction of the seismic belt and are close to the direction of the Heze fault (Zhang et al., 1990a, 1990b). As indicated by Zhang et al. (1990a, 1990b), this direction is also along the direction of the primary rupture plane of the Heze M 5.9 earthquake (i.e., NW with azimuth 114°). Figure 12 displays the primary rupture directions of the other small and medium earthquakes that occurred in the same area during the normal periods. No obvious difference is seen in the rupture directions shown in Figures 10 and 11.

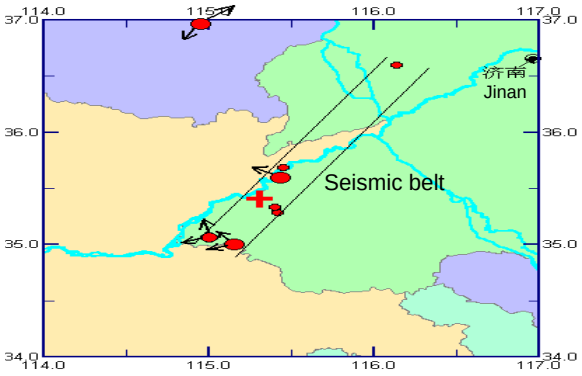

Fig. 10 Primary rupture directions of small and medium earthquakes that occurred on the seismic belt before the Heze M 5.9 earthquake

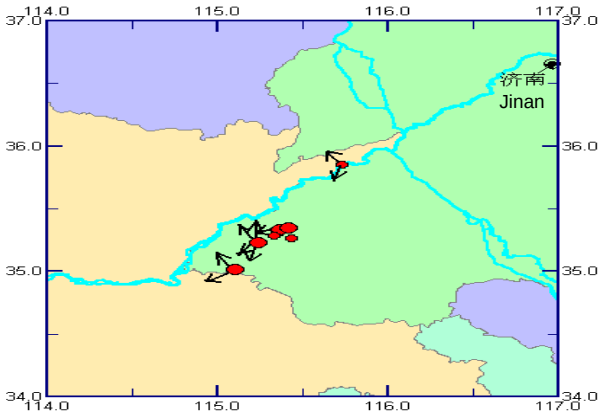

Fig. 11 Primary rupture directions of small and medium earthquakes that occurred during the normal periods in the Heze area

3.2 Calculation of Ambient Shear Stress, Temporal Periodicity of Waveform, Q Value and Width of Fourier Spectrum

Table 4 lists the ambient shear stress τ, the temporal periodicity of waveform, r, Q value, and the width of Fourier spectrum, w, of the small and medium earthquakes that occurred during the Heze M 5.9 earthquake sequence. Figure 12 shows the variation of ambient shear stress during the Heze M 5.9 earthquake sequence. From this figure and Table 4, it can be seen that similar to the Liyang earthquake, the shear stress had more and higher peak values and varied more violently before the Heze M 5.9 earthquake. As shown in Table 4, during the year and half preceding the Heze earthquake, the mean stress value was 45.17 bar with the standard deviation of 52.92 bar, and after the earthquake, the mean stress value dropped to 24.74 bar and the standard deviation became 54.85 bar. While after the earthquake, the shear stress value stayed at a lower level, it varied smoothly. It is also observed that there are two earthquakes whose shear stress values were much higher than the others. Those earthquakes are (i) the M 4.6 earthquake that occurred on December 23, 1981 and whose τ value was 170.7 bar, and (ii) the M 4.8 earthquake that occurred on May 29, 1982 and whose τ value was 104.1 bar. Both earthquakes were the cases of unilateral rupture, with the L_0/L value equal to 1.0. The M 4.6 earthquake occurred two years before the Heze earthquake and its epicentral distance was only 50 km. Further, until the occurrence of the Heze earthquake, this was the strongest earthquake that had occurred within a 100-km radius and the second strongest earthquake that had occurred within a 200-km radius. Therefore, the M 4.6 earthquake is considered as the foreshock of the Heze earthquake.

Table 4: τ, r, Q, w of Small and Medium Earthquakes That Occurred during Heze M 5.9 Earthquake Sequence

No.	Date	Time	Longitude	Latitude	M_L	τ (bar)	r ($\times 10^{-1}$)	Q_2	w (Hz)
Before Heze M 5.9 earthquake									
1	1981-12-23	06:27	115°26’	35°36’	4.6	170.7	9.98	287	0.66
2	1982-01-17	14:57	115°00’	35°04’	3.1	7.1	9.93	282	0.52
3	1982-01-22	23:19	116°08’	36°36’	2.5		9.97		
4	1982-04-09	08:31	115°27’	35°41’	2.1		9.88		
5	1982-05-29	18:28	114°57’	36°58’	4.8	104.1	9.98	260	0.87
6	1982-07-21	19:33	115°25’	35°17’	2.6	1.7	9.99	301	0.25
7	1982-07-26	10:34	115°24’	35°20’	2.4		9.90		
8	1982-07-28	01:23	115°09’	35°00’	4.0	29.7	9.98	353	0.53
After Heze M 5.9 earthquake									
9	1990-02-20	19:49	115°14’	35°14’	3.0	7.2	9.98	354	0.65
10	1990-06-18	09:18	115°21’	35°18’	2.5		9.85		
11	1990-07-12	07:39	115°22’	35°20’	3.0	11.0	9.97	487	0.62
12	1991-11-11	03:09	115°06’	35°01’	3.2	10.5	9.98	437	0.95
13	1993-12-03	03:49	115°25’	35°21’	3.0	9.6	9.96	427	0.80
14	1994-08-28	22:04	115°26’	35°16’	2.6	2.0	9.94	310	0.89
15	1995-02-16	21:35	115°20’	35°17’	2.6	2.2	9.95	344	0.28
16	1995-04-14	10:56	115°44’	35°51’	2.7	2.4	9.97	323	0.14

Figure 13 shows the variation of the temporal periodicity of waveform, r. From this figure and Table 4, it is seen that r varied smoothly between 0.99 and 1.00. Due to the missing of earthquake samples that occurred during the year preceding the Heze earthquake (i.e., from November, 1982 to November, 1983), no violent variation has been observed in r during the Heze earthquake sequence.

The variations of Q_2 and width of Fourier spectrum, w, are displayed in Figures 14 and 15, respectively. These figures show that there were no obvious differences in the variations of Q_2 and w before and after the Heze earthquake.

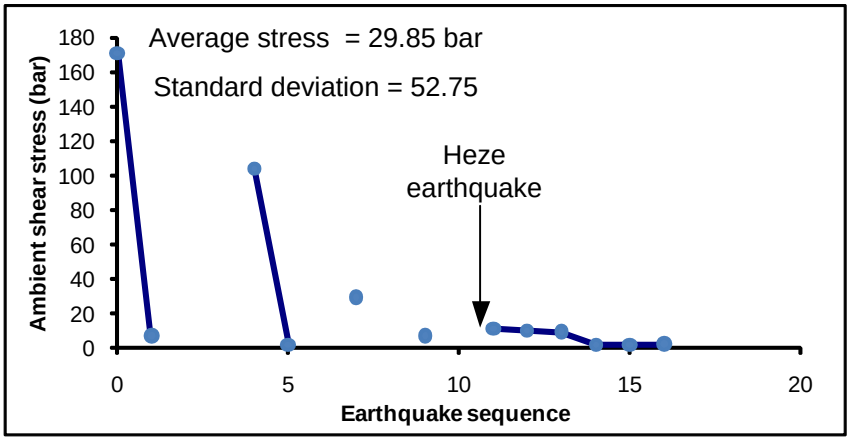

Fig. 12 Ambient shear stress τ of small and medium earthquakes in the Heze M 5.9 earthquake sequence

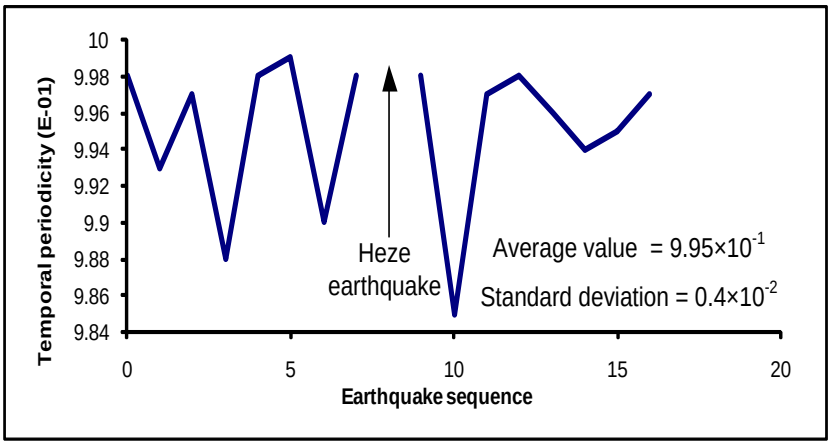

Fig. 13 Temporal periodicity of waveform, r, of small and medium earthquakes in the Heze M 5.9 earthquake sequence

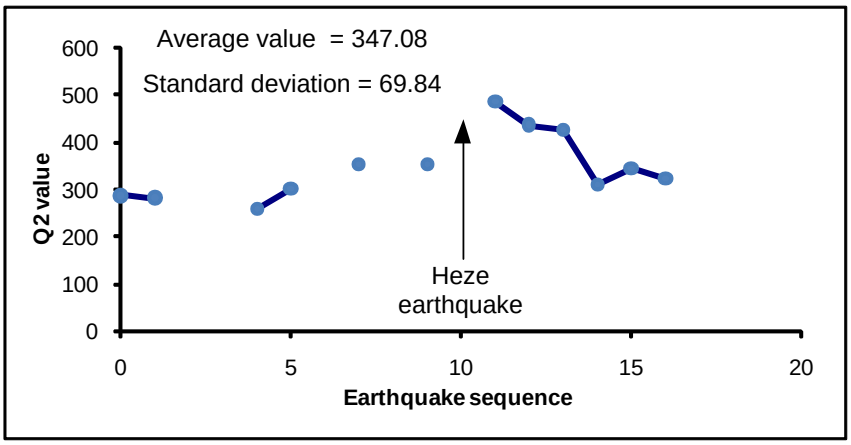

Fig. 14 Q_2 values of the P-waves of small and medium earthquakes in the Heze M 5.9 earthquake sequence

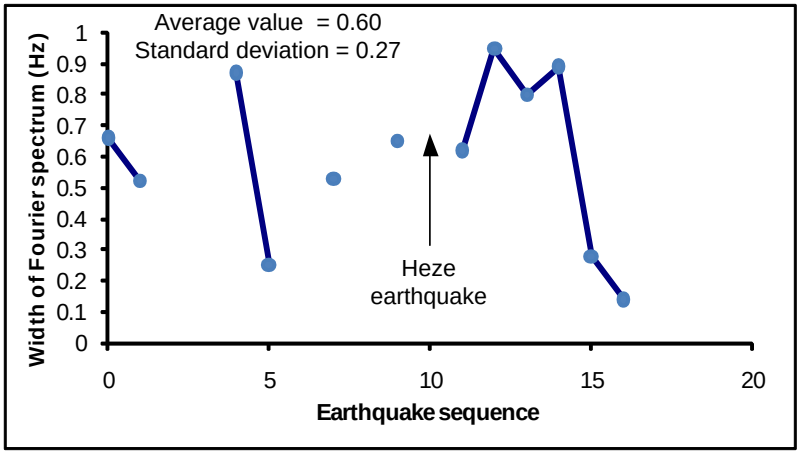

Fig. 15 Fourier spectral width w of small and medium earthquakes in the Heze M 5.9 earthquake sequence

3.3 Discussion on Heze M 5.9 Earthquake

Based on the analysis of the above data, following conclusions are drawn for the Heze earthquake sequence:

1. The primary rupture directions of the earthquakes that occurred on the Heze seismic belt are conjugated to the direction of the belt and are close to the direction of the Heze fault. These directions also coincide with the direction of the primary rupture plane of the Heze M 5.9 earthquake (Zhang et al., 1990a, 1990b).
2. A few of the high ambient shear stress values and turbulent variations in the shear stress took place during the period of year and a half preceding the main shock, and in other times, the shear stress was lower and varied smoothly. As shown in Table 4, during the year preceding the Heze earthquake, the mean stress value was 45.17 bar with the standard deviation of 52.92 bar, while after that earthquake, the mean stress value dropped to 24.74 bar and the standard deviation became 54.85 bar. The phenomenon of higher ambient shear stress before the Heze earthquake is also reflected in the median value of the ambient shear stress. The median stress value in the period of year and a half preceding the main shock was 29.7 bar, as against 7.2 bar during the other times. This proves that in the case of the Heze earthquake, the ambient shear stress was much higher before the main shock compared to that after the main shock.
3. The value of the temporal periodicity of waveform, r, was high and it varied smoothly in the range 0.99±0.01. Due to the missing of the earthquake samples that occurred in the year preceding the Heze earthquake (i.e., from November, 1982 to November, 1983), there was neither a violent variation nor a low value in r was observed.
4. The M 4.6 earthquake occurred two years before the Heze earthquake (i.e., on December 23, 1981) and its epicentral distance was 50 km. Until the occurrence of the Heze earthquake, this was the strongest earthquake that had occurred within a 100-km radius and the second strongest one that had occurred within a 200-km radius. Therefore, this earthquake is considered as the foreshock of the Heze earthquake. Similarly, the ambient shear stress τ (= 170.7 bar) for this earthquake (i.e., the foreshock) was much higher than the other stress values.
5. The earthquakes that occurred before the main shock were closer to a unilateral rupture than the earthquakes that occurred after it. The median r for the four events before the main shock is 0.95, and for the six events afterwards this is 0.90. However, such a difference in r is not obvious, and the mean r is 0.91 for the four events before the main shock and 0.89 for the six events afterwards.
6. No regularity has been evident in the variations of the Q values for P-waves and the width of Fourier spectrum before and after the Heze M 5.9 earthquake.

4. Analysis of Southern Yellow Sea M 6.2 Earthquake

4.1 Analysis of Rupture Characteristics

Table 5 lists the calculated results on the rupture characteristics of the medium and small earthquakes that occurred before and after the southern Yellow Sea M 6.2 earthquake. From this table, the average L_0/L value of thirteen earthquakes that occurred before the southern Yellow Sea earthquake is calculated as 0.92. Among these earthquakes, five earthquakes had the L_0/L value of 1.0, five earthquakes had the L_0/L value between 0.90 and 0.99, two earthquakes had the L_0/L value between 0.80 and 0.89, and one earthquake had the L_0/L value between 0.70 and 0.79. The average L_0/L value of the four earthquakes that occurred after the southern Yellow Sea earthquake is 0.90. For two of these earthquakes, the L_0/L values are located between 0.90 and 0.99 and for the other two earthquakes, the L_0/L values are located between 0.80 and 0.89. Comparatively, the earthquakes that occurred before the main shock were a little bit closer to the case of unilateral rupture than the earthquakes that occurred after the main shock, but such a difference was not supported by the other results. This implies that the occurrence of small earthquakes with unilateral rupture is not sufficient but only a necessary condition for the medium and strong earthquakes to occur.

Table 5: Rupture Characteristics of Medium and Small Earthquakes That Occurred before and after Southern Yellow Sea M 6.2 Earthquake

No.	Date	Time	Longitude	Latitude	M_L	L_0/L	λ_1, σ_1 (°)	λ_2, σ_2 (°)	n	CF
Before southern Yellow Sea M 6.2 earthquake										
1	1978-07-06	11:44	120°57’	32°43’	3.7	1.0	14.8, 0	134.8, 0	4	III
2	1978-07-17	22:48	120°50’	32°45’	3.9	0.90	47.4, 8.5	138.9, 8.8	5	III
3	1979-01-04	18:28	120°30’	33°50’	4.3	1.0	120.7, 5.8		4	I
4	1981-01-11	21:30	120°36’	33°34’	3.7	0.95	155.9, 5.2	220.9, 5.2	7	III
5	1983-09-10	07:47	122°29’	34°14’	3.5	0.73			5	
6	1983-09-25	14:30	120°07’	32°51’	3.5	0.94	238.8, 11.6		9	I
7	1983-10-07	19:38	122°19’	34°26’	3.7	0.80	229.4, 17.3		3	II
8	1983-10-11	22:36	121°20’	34°35’	3.9	1.0	313.9, 4.3	220.5, 4.3	10	III
9	1983-10-14	05:00	121°16’	34°40’	3.3	1.0	313.9, 15	223.9, 15	4	III
10	1983-10-19	14:25	121°25’	33°49’	4.1	0.96	233.3, 12.4		8	I
11	1984-05-16	17:16	120°35’	33°05’	3.6	0.93	213.7, 14.0		7	I
12	1984-05-17	11:56	120°30’	33°05’	3.3	1.0	36.1, 13.2	221.1, 22.9	6	III
13	1984-05-17	11:59	120°30’	33°05’	3.4	0.80	198.6, 7.5	333.6, 7.5	4	III
After southern Yellow Sea M 6.2 earthquake										
14	1992-05-29	16:33	120°38’	33°29’	3.3	0.93	226.8, 15	24.3, 22.5	4	III
15	1992-08-19	07:49	120°58’	33°40’	3.0	0.97	25.7, 15		4	I
16	1992-08-25	03:21	121°42’	34°12’	4.1	0.86	232.6, 11.2			I
17	1992-10-25	17:46	120°34’	32°45’	3.5	0.83	135.4, 8.6		12	I

Figure 16 shows the primary rupture directions of the small and medium earthquakes on the seismogenic zone that occurred before the southern Yellow Sea earthquake. From this figure, it is observed that the candidate primary rupture directions are either tangent to the edge of the gap or are

pointing outside the gap. Such characteristics are very similar to those of the earthquakes that occurred on the Liyang seismic gap.

Figure 17 displays the primary rupture directions of the small and medium earthquakes that occurred on the seismic belt before the southern Yellow Sea earthquake. From this figure, it is seen that most primary rupture directions are consistent with the direction of this seismic belt and are pointed south-west (SW) except for the following three earthquakes: the M_L 3.3 earthquake that occurred at 11:56 hours on May 17, 1984; the M_L 3.4 earthquake that occurred at 11:59 hours on May 17, 1984; and the M_L 3.3 earthquake that occurred at 5:00 hours on October 14, 1983. Each of the three earthquakes have two candidate primary rupture directions and one of those directions is pointed SW. The other rupture direction of the first earthquake is pointed northeast (NE), and the other rupture directions of the other two earthquakes is pointed northwest (NW) and is conjugated to the direction of this seismic belt. As stated in Chen et al. (2002), for this seismic belt, the azimuth of the nodal plane 1 is 350° and the azimuth of the nodal plane 2 is 77°. Based on the distribution of the plotted primary rupture directions, the nodal plane 2 is determined to be the primary rupture plane that extends in the north-east (NE) direction.

The primary rupture directions of the small and medium earthquakes that occurred in the same area (i.e., the seismic belt for the southern Yellow Sea earthquake) during the normal periods are plotted in Figure 18. These directions point either SW or NE, which is approximately consistent with the direction of the belt.

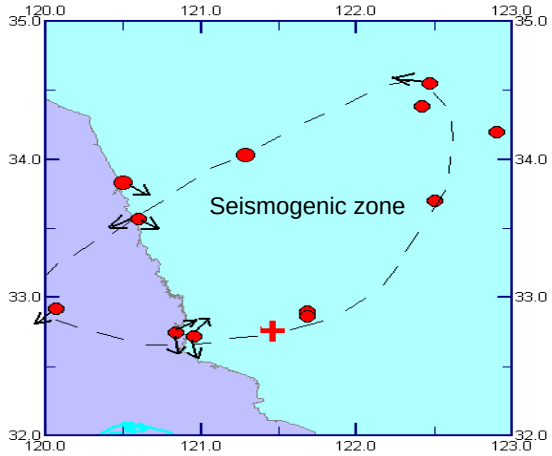

Fig. 16 Primary rupture directions of small and medium earthquakes on the seismogenic zone of the southern Yellow Sea M 6.2 earthquake

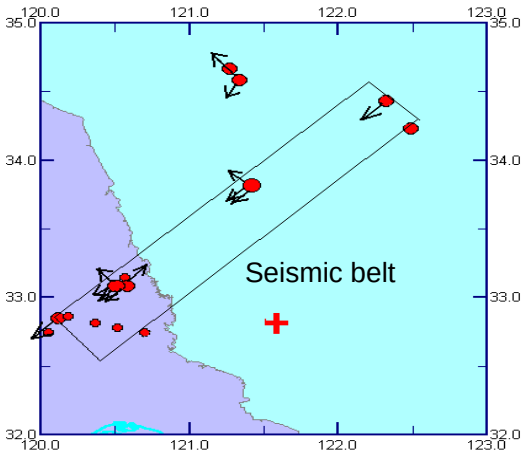

Fig. 17 Primary rupture directions of small and medium earthquakes that occurred on the seismic belt before the southern Yellow Sea M 6.2 earthquake

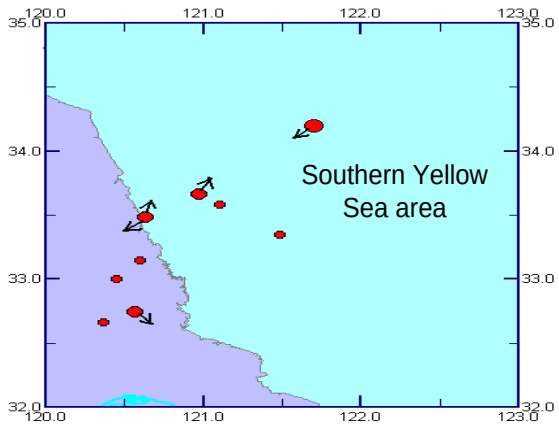

Fig. 18 Primary rupture directions of small and medium earthquakes that occurred during the normal periods in the southern Yellow Sea area

4.2 Calculation of Ambient Shear Stress, Temporal Periodicity of Waveform, Q Value and Width of Fourier Spectrum

The ambient shear stress τ, the temporal periodicity of waveform, r, Q value, and the width of Fourier spectrum, w, of the small and medium earthquakes that occurred before and after the southern Yellow Sea M 6.2 earthquake are listed in Table 6.

Table 6: τ, r, Q, w of Small and Medium Earthquakes That Occurred during the Southern Yellow Sea M 6.2 Earthquake Sequence

No.	Date	Time	Longitude	Latitude	M_L	τ (bar)	r ($\times 10^{-1}$)	Q_1	Q_2	w (Hz)
Before southern Yellow Sea M 6.2 earthquake										
1	1975-12-30	12:00	121°17’	34°02’	4.3	8.6	9.99			5.10
2	1976-04-15	00:19	121°41’	32°54’	3.7	19.3	9.96		545	0.42
3	1977-02-21	18:21	122°28’	34°33’	3.8	16.2	9.99			0.39
4	1977-06-09	00:49	122°25’	34°23’	3.6	3.4	9.94		445	1.59
5	1977-07-25	05:25	122°30’	33°42’	3.6	4.0	9.99		451	0.42
6	1978-01-24	04:16	122°54’	34°12’	3.8	29.7	9.91			0.26
7	1978-07-06	11:44	120°57’	32°43’	3.7	41.0	9.98			2.91
8	1978-07-17	22:48	120°50’	32°45’	3.9	53.0	9.92		513	2.56
9	1979-01-04	18:28	120°30’	33°50’	4.3	49.0	9.92		511	0.10
10	1979-04-16	18:49	121°41’	32°52’	3.6	9.4	9.98		477	0.40
11	1981-01-11	21:30	120°36’	33°34’	3.7	46.8	9.98		482	1.70
12	1983-09-10	07:47	122°29’	34°14’	3.5	9.3	9.97			2.32
13	1983-09-25	14:30	120°07’	32°51’	3.5	11.1	9.99		549	0.74
14	1983-10-07	19:38	122°19’	34°26’	3.7	50.9	9.97		689	1.60
15	1983-10-11	22:36	121°20’	34°35’	3.9	67.0	9.99		492	1.49
16	1983-10-14	05:00	121°16’	34°40’	3.3	13.0	9.99		393	2.03
17	1983-10-19	14:25	121°25’	33°49’	4.1	57.6	9.97			2.71
18	1983-11-20	08:15	120°03’	32°45’	2.2	2.8	9.98			1.04
19	1984-03-07	23:10	120°22’	32°49’	2.5		9.63			
20	1984-03-20	04:01	120°42’	32°45’	2.5	2.3	9.83	209	302	0.45
21	1984-03-20	04:01	120°31’	32°47’	2.8	5.7	9.94		257	
22	1984-05-11	11:37	120°11’	32°52’	2.5	1.3	9.98		306	0.23
23	1984-05-15	22:52	120°34’	33°09’	2.7		9.96			
24	1984-05-16	17:16	120°35’	33°05’	3.6	7.9	9.98		521	2.60
25	1984-05-17	11:56	120°30’	33°05’	3.3	10.6	9.97		551	2.89
26	1984-05-17	11:59	120°30’	33°05’	3.4	9.9	9.98		487	1.36
After southern Yellow Sea M 6.2 earthquake										
27	1992-01-27	18:34	120°22’	32°40’	2.5	2.0	9.98		316	3.97
28	1992-02-08	07:46	121°06’	33°35’	2.6		9.86			
29	1992-03-12	06:13	120°27’	33°00’	2.8	15.1	9.99		353	3.80
30	1992-05-29	16:33	120°38’	33°29’	3.3	11.8	9.88		424	3.38
31	1992-08-19	07:49	120°58’	33°40’	3.0	12.1	9.94		446	2.20

32	1992-08-20	05:05	121°29’	33°21’	2.9	11.0	9.99		499	1.93
33	1992-08-25	03:21	121°42’	34°12’	4.1	47.4	9.99		617	1.71
34	1992-10-13	17:59	120°06’	34°12’	2.6	1.9	9.86		331	1.48
35	1992-10-25	17:46	120°34’	32°45’	3.5	9.5	9.98		486	2.73

Figure 19 shows the variation of ambient shear stress during the southeastern Yellow Sea M 6.2 earthquake sequence. Similar to the above two examples, it is found that the peak value of τ was higher and that the stress itself varied violently, especially during the eight months preceding the M 6.2 earthquake. During the other periods, the τ value was low and varied smoothly.

Figure 20 displays the variation of the temporal periodicity of waveform, r. From this figure and Table 6, it is seen that the temporal periodicity r varied smoothly within the range 0.99±0.01 during the normal time periods and that it reached the lowest value of 0.963 two months before the main shock.

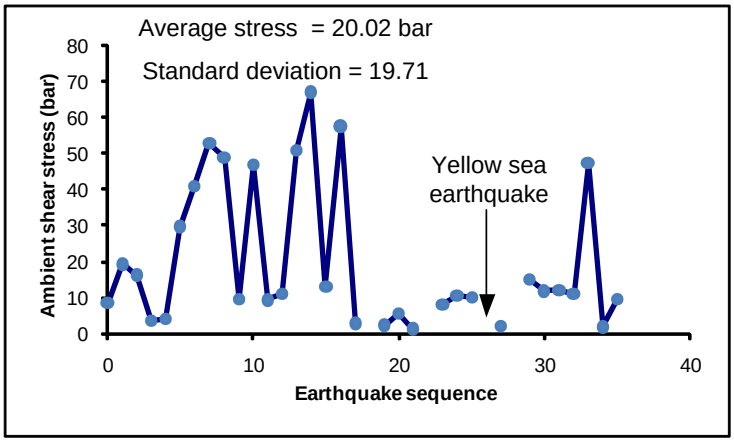

Fig. 19 Ambient shear stress τ of small and medium earthquakes in the southern Yellow Sea M 6.2 earthquake sequence

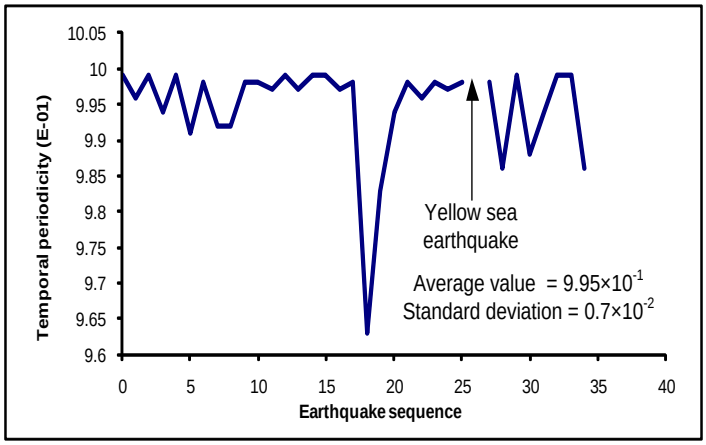

Fig. 20 Temporal periodicity of waveform, r, of small and medium earthquakes in the southern Yellow Sea M 6.2 earthquake sequence

Figures 21 and 22 respectively show the variations of Q_2 and the width of Fourier spectrum, w. From these variations, it is observed that there were no obvious differences in the variations of Q_2 and w before and after the southern Yellow Sea M 6.2 earthquake.

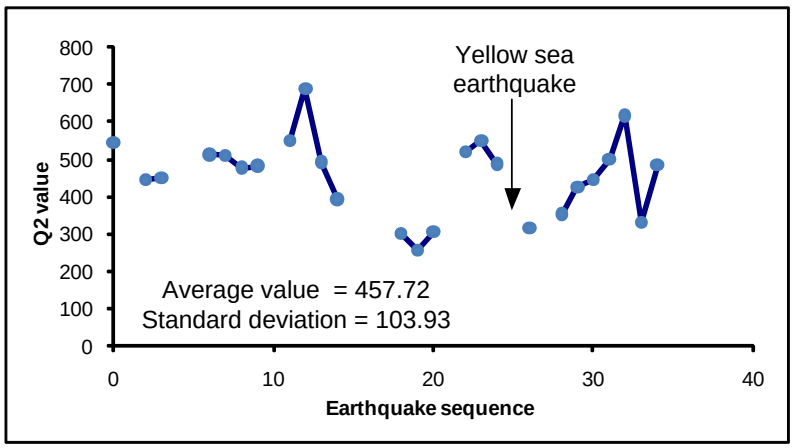

Fig. 21 Q_2 values of the P-waves of small and medium earthquakes in the southern Yellow Sea M 6.2 earthquake sequence

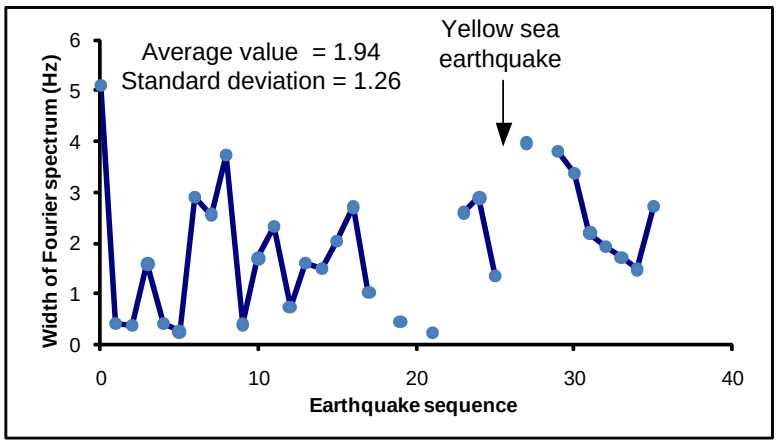

Fig. 22 Fourier spectral width w of small and medium earthquakes in the southern Yellow Sea M 6.2 earthquake sequence

4.3 Discussion on Southern Yellow Sea M 6.2 Earthquake

Based on the analysis of the above data, the following conclusions are drawn for the southern Yellow Sea earthquake sequence:

1. The primary rupture directions of the earthquakes that occurred on the seismogenic zone were parallel to the nodal plane of the following main shock, and they were either tangent to the zone or pointing towards outside the zone. However, during the normal periods, these directions were disorganized.
2. The primary rupture directions of the earthquakes that occurred on the seismic belt were close to the direction of the belt and were pointed SW. For an earthquake that occurred during the normal periods, the primary rupture direction was pointed SW or NE.
3. A few high values of ambient shear stress and turbulent variations in the shear stress were observed during the eight months preceding the main shock, while in other times, the shear stress value was lower and varied smoothly. According to Table 6, within the period of eight months preceding the main shock, the mean stress value was 25.17 bar with the standard deviation of 22.49 bar, while during the other times, the mean stress value was 12.48 bar and the standard deviation became 11.87 bar. However, the median stress value in the period of eight months preceding the main shock was only 9.9 bar and that value during the other times was 12.1 bar. Considering that the peak stress value before the main shock (i.e., 67 bar) is much higher than the peak stress during the other times (i.e., 53 bar), this phenomenon has accounted for the severe change in the ambient shear stress values before the main shock.

4. The temporal periodicity of waveform, r, changed violently and there was one really low value (of 0.96) observed within the period of two months before the main shock. During the normal periods, r varied smoothly within the range 0.99±0.01.
5. The earthquakes that occurred before the main shock were a little bit closer to a unilateral rupture than the earthquakes that occurred after it, but such a difference in L_0/L is not obvious. As shown in Table 5, the median r for the 13 events before the main shock is 0.95, and for the four events afterwards this is 0.90. However, such a difference in r is not obvious, and the mean r is 0.92 for the 13 events before the main shock and 0.90 for the four events afterwards.
6. There has been no obvious regularity in the variations for the Q values of P-waves and the widths of Fourier spectra before and after the southern Yellow Sea M 6.2 earthquake.

5. Analysis of M 6.1 and M 6.2 Earthquakes in Northern Gulf

5.1 Analysis of Rupture Characteristics

The rupture characteristics of the medium and small earthquakes that occurred before and after the northern Gulf earthquakes are shown in Table 7. From this table, the average L_0/L value of the eleven small and medium earthquakes preceding the northern Gulf earthquakes is obtained as 0.91 and the average L_0/L value of the five earthquakes that occurred afterwards is obtained as 0.89. Comparatively, the earthquakes that occurred before the main shocks were closer to a unilateral rupture than the earthquakes that occurred after the main shocks, but this difference was not supported by the other results.

Table 7: Rupture Characteristics of Medium and Small Earthquakes That Occurred before and after the Northern Gulf M 6.1, M 6.2 Earthquakes

No.	Date	Time	Longitude	Latitude	M_L	L_0/L	λ_1, σ_1 (°)	λ_2, σ_2 (°)	n	CF
Before northern Gulf M 6.1, M 6.2 earthquakes										
1	1991-03-09	12:45	110°46’	21°12’	2.9	1.0			2	
2	1992-01-12	10:42	109°42’	20°51’	2.1	1.0			2	
3	1992-10-28	10:13	109°50’	21°22’	2.6	1.0			2	
4	1993-02-22	03:49	110°52’	19°42’	2.9	1.0	344.4, 0		3	I
5	1993-03-05	04:29	109°30’	21°20’	2.8	1.0			2	
6	1993-10-11	10:58	107°55’	21°52’	2.7	0.75			3	
7	1994-02-12	09:24	109°42’	21°55’	3.4	1.0			3	
8	1994-09-06	22:27	110°29’	21°03’	2.4	0.70			2	
9	1994-10-02	19:34	108°24’	20°53’	2.8	0.60			2	
10	1994-10-24	10:10	110°28’	20°50’	3.1	1.0	60.4, 13.2		5	I
11	1994-12-28	15:26	108°32’	21°36’	2.8	1.0			2	
After northern Gulf M 6.1, M 6.2 earthquakes										
12	1999-03-12	18:37	109°24’	20°33’	2.8	1.0			2	
13	1999-06-06	09:54	109°52’	20°58’	2.9	1.0	50.3, 22.9		3	II
14	1999-06-30	16:41	109°22’	20°34’	3.2	0.72	234.1, 22.9	54.1, 22.9	6	III
15	1999-07-06	16:46	110°14’	20°32’	3.6	0.90	214.4, 17.3		5	II
16	1999-10-30	04:31	110°31’	20°52’	3.2	0.83			5	

In this area, there are only a few earthquakes whose primary rupture directions have been determined. Those primary rupture directions are close to each other and point either SW or NE (see Figure 23). As stated by Chen et al. (2002), no seismogenic zone or seismic belt had been found in this area before the northern Gulf M 6.1 and M 6.2 earthquakes.

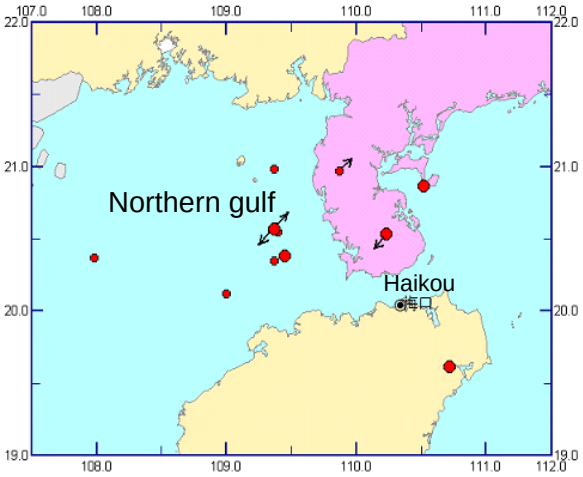

Fig. 23 Primary rupture directions of small and medium earthquakes that occurred during the normal periods in northern Gulf area

5.2 Calculation of Ambient Shear Stress, Temporal Periodicity of Waveform, Q Value and Width of Fourier Spectrum

The ambient shear stress τ, the temporal periodicity of waveform, r, Q value, and the width of Fourier spectrum, w, of the small and medium earthquakes that occurred before and after the northern Gulf M 6.1 and M 6.2 earthquakes are listed in Table 8.

Table 8: τ, r, Q, w of Small and Medium Earthquakes That Occurred during the Northern Gulf M 6.1 and M 6.2 Earthquakes Sequence

No.	Date	Time	Longitude	Latitude	M_L	τ (bar)	r ($\times 10^{-1}$)	Q_1	Q_2	w (Hz)
Before northern Gulf M 6.1, M 6.2 earthquakes										
1	1991-03-09	12:45	110°46’	21°12’	2.9	16.2	9.82	111	267	0.31
2	1991-05-03	14:55	108°42’	21°05’	3.1	12.7	9.82		289	0.37
3	1991-06-21	05:50	109°40’	20°49’	2.6		9.67			
4	1991-10-29	01:55	108°05’	21°38’	2.4		9.68			
5	1992-01-12	10:42	109°42’	20°51’	2.1	2.0	9.82	91		0.36
6	1992-10-04	04:52	108°36’	19°55’	2.7	2.0	9.95		424	0.12
7	1992-10-28	10:13	109°50’	21°22’	2.6	1.7	9.89	99	141	0.18
8	1992-12-16	03:22	108°28’	21°21’	2.2	2.8	9.96	276		0.16
9	1993-01-13	18:20	108°34’	21°42’	2.2		9.39			
10	1993-02-22	03:49	110°52’	19°42’	2.9	12.7	9.98		262	0.48
11	1993-03-05	04:29	109°30’	21°20’	2.8	10.6	9.97	191	217	0.20
12	1993-03-13	18:04	108°38’	21°47’	2.3		9.61			
13	1993-06-25	18:54	108°37’	21°44’	2.2		9.87			
14	1993-10-11	10:58	107°55’	21°52’	2.7	2.0	9.97		196	0.30
15	1994-01-02	19:34	108°24’	20°53’	2.8	13.4	9.92		359	0.41
16	1994-02-12	09:24	109°42’	21°55’	3.4	9.1	9.97	238	449	0.21
17	1994-09-06	22:27	110°29’	21°03’	2.4	2.3		72	187	0.27
18	1994-10-24	10:10	110°28’	20°50’	3.1	11.5	9.97	94	287	0.43

19	1994-12-28	15:26	108°32’	21°36’	2.8	15.4	9.93		412	0.34
After northern Gulf M 6.1, M 6.2 earthquakes										
20	1999-01-02	16:09	107°59’	20°22’	2.6		9.59			
21	1999-03-12	18:37	109°24’	20°33’	2.8	12.1	9.84		219	0.22
22	1999-05-19	11:07	109°22’	20°59’	2.5		9.58			
23	1999-06-06	09:54	109°52’	20°58’	2.9	12.9	9.83		282	0.23
24	1999-06-30	16:41	109°22’	20°34’	3.2	10.8	9.96		356	0.26
25	1999-07-06	16:46	110°14’	20°32’	3.6	9.9	9.99		396	0.40
26	1999-08-29	03:42	109°27’	21°23’	3.0	13.2	9.94		267	0.22
27	1999-08-31	16:29	109°00’	20°07’	2.7	2.0	9.93		199	0.44
28	1999-10-25	17:46	120°34’	32°45’	3.5	9.5	9.98		486	2.73
29	1999-10-30	04:31	110°31’	20°52’	3.2	12.1	9.97		369	0.17
30	1999-12-10	06:11	110°43’	19°37’	3.1	12.7	9.93		323	0.12
31	1999-12-11	21:53	109°22’	20°21’	2.5	2.5	9.93		198	0.23

Figure 24 shows the variation of ambient shear stress τ in the northern Gulf M 6.1 and M 6.2 earthquake sequence. Similar to the previous samples, it is observed that the shear stress had more and higher peak values and that it varied violently during the year preceding the M 6.1 and M 6.2 earthquakes. However, during the other time periods, the shear stress remained low and varied smoothly.

Figure 25 shows the variation of the temporal periodicity of waveform, r, in the northern Gulf earthquake sequence. From this figure, it is observed that the temporal periodicity r was on the higher side and varied smoothly during most of the normal time periods (except during the first four earthquakes following the northern Gulf earthquakes), while it reached the lowest value of 0.939 and varied violently during the two years preceding the M 6.1 and M 6.2 earthquakes.

Figures 26–28 show the variations of Q values and the width of Fourier spectrum, w. From these figures, it is observed that similar to the previous samples, there are no obvious differences in the variations of Q_1, Q_2 and w before and after the northern Gulf M 6.1 and M 6.2 earthquakes. The fact that the Q_2 values are higher than the Q_1 values again proves that the quality factors for a deep medium are higher than those for a shallow medium.

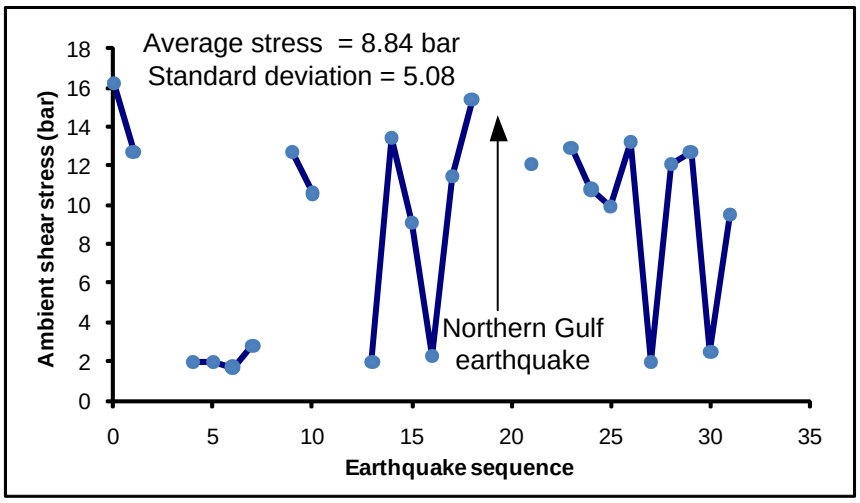

Fig. 24 Ambient shear stress τ of small and medium earthquakes in the northern Gulf M 6.1 and M 6.2 earthquakes sequence

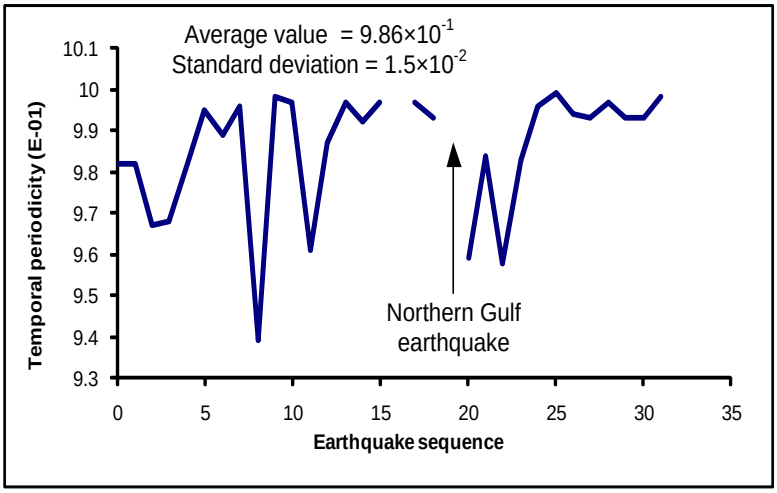

Fig. 25 Temporal periodicity of waveform, r, of small and medium earthquakes in the northern Gulf M 6.1 and M 6.2 earthquakes sequence

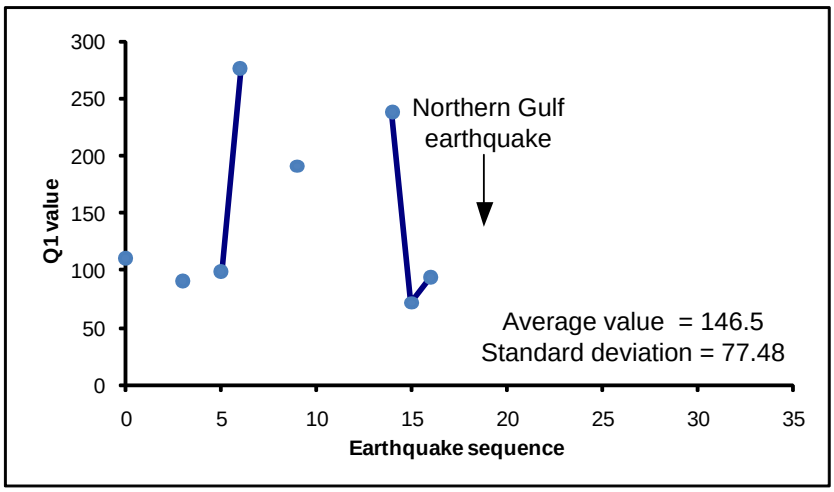

Fig. 26 Q_1 values of the P-waves of small and medium earthquakes in the northern Gulf M 6.1 and M 6.2 earthquakes sequence

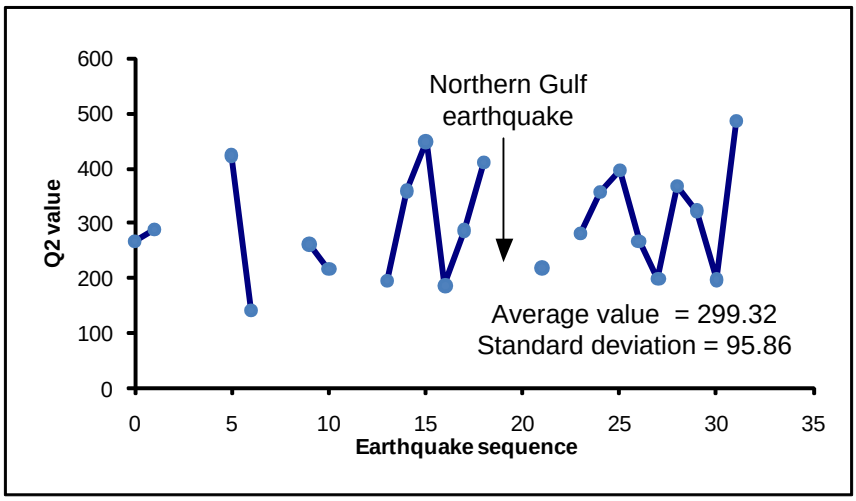

Fig. 27 Q_2 values of the P-waves of small and medium earthquakes in the northern Gulf M 6.1 and M 6.2 earthquakes sequence

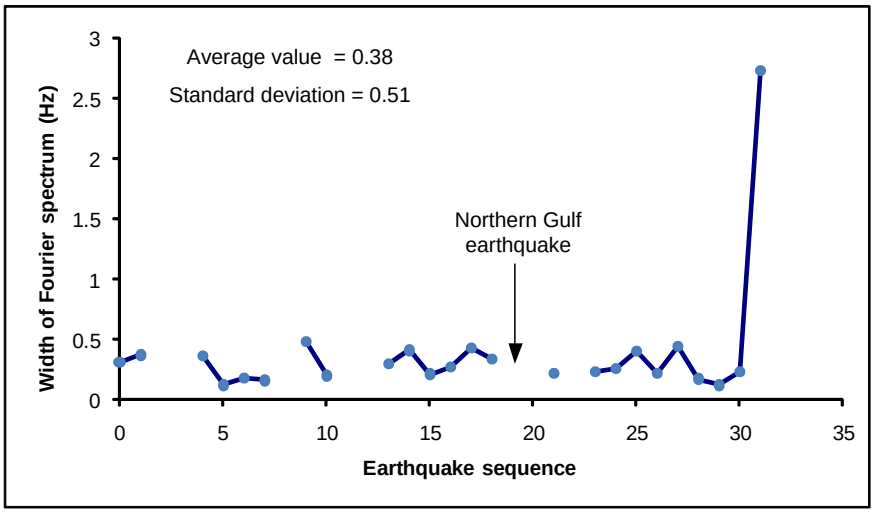

Fig. 28 Fourier spectral width w of small and medium earthquakes in the northern Gulf M 6.1 and M 6.2 earthquakes sequence

5.3 Discussion on Northern Gulf M 6.1 and M 6.2 Earthquakes

On investigating the parameters listed in Tables 7 and 8, following observations have been made for the northern Gulf earthquake sequence:

1. The primary rupture directions of the earthquakes that occurred in the northern Gulf area were close to each other and were pointed SW or NE.
2. A few of the high ambient shear stress values were observed before the main shocks. The mean stress value was 10.34 bar with the standard deviation of 5.70 bar during the year preceding the main shocks, while during the other times, the mean stress value was 8.44 bar and the standard deviation was 4.16 bar. This trend was even reflected in the median stress values, with the median stress value being 11.5 bar during the year preceding the main shocks and 10.6 bar during the other times.
3. The temporal periodicity of waveform, r, changed a little bit more evidently and several lower values of r were observed within the period of two years preceding the main shocks. The minimum value observed was 0.939. However, r varied smoothly during the normal time periods. Whereas the standard deviation of r was 0.02 within the two-year period before the main shocks, this was only 0.013 in the other times.
4. The earthquakes that occurred before the main shocks were closer to a unilateral rupture (i.e., L_0/L was closer to 1.0) than the earthquakes that occurred after them, but such a difference in L_0/L is not obvious. From Table 7, the median r for the 11 events before the main shocks is obtained as 1, and for the five events afterwards this is obtained as 0.9. However, such a difference in r is not obvious, and the mean r is 0.91 for the 11 events before the main shocks and 0.89 for the four events afterwards.
5. No regularity has been evident in the variations of the Q values of P-waves and the width of Fourier spectrum before and after the northern Gulf M 6.1 and M 6.2 earthquakes. Also, it has not been possible to obtain the Q values after the main shocks because (1) most aftershocks were small earthquakes and could only be detected by local seismic stations, and the analog records mixed with P waves could hardly be used for digitization and spectral analysis, (2) in a certain amount of time after the main shocks and within the area around the epicenter, the ambient stress and Q values were in a severe adjustment disorder and it was impossible to use one data to represent the Q value in the whole area.

ERROR ESTIMATION

1. Errors in Determining Rupture Directions

1.1 Errors Caused by Digitization

Digitization is the representation of an original analog record $f(t)$ by a discrete set of points sampled at an equal time interval. The maximum error caused by this discretization, Δf, is

$$\Delta f = \frac{(\Delta t)^2}{8}\left| f''(x)\right|_{\max} + \frac{A}{2} \tag{20}$$

where A is the digitization precision (~ 0.05 mm). The resolution ratio of the scanner is 300 dpi and the dot pitch is 0.085 mm. On using Equation (20), it can be estimated that in our study, the error caused by the discretization Δf is about 1.1%.

1.2 Errors Caused by Simplified Hypocenter and Medium Model

In the asymmetric bilateral rupture model used in our studies, it is assumed that the focal depth is zero. Therefore, the radiation pattern factor R_α is simplified as $R_\alpha = \sin 2\theta \cos\varphi = \sin 2\theta.$ If the actual focal depth is 15 km and the epicentral depth is 200 km, we have φ = $\tan^{-1}$(15/200) and thus R_α = $\sin 2\theta \cos\varphi$ = $0.9972 \sin 2\theta.$ The relative error in this estimate is only 0.28%. Also, other errors caused by the uneven distribution of the quality factor (i.e., Q value) of the medium are eliminated because the generalized directional function is a ratio between two spectra.

1.3 Errors Generated in Plotting Generalized Directional Function Curves

As mentioned before, in determining the primary rupture directions of the above earthquake samples, we have chosen twelve θ values from 0º to 180º with the equal increment of 15º to calculate and plot the generalized directional function curves. This implies that the maximum error generated in the above process could be 15°, which is the major factor that causes errors in measuring rupture directions.

2. Errors in Evaluating Ambient Stress τ

In evaluating the ambient stress τ, it has been assumed that the average stress field is reduced to zero after an earthquake and that the yield strength of crust is the value of 200 MPa measured in laboratory. Besides the above assumptions, the precision in determining ambient stress is also influenced by the surface wave magnitude m_s and the hypocentral radius r_h.

2.1 Influence of m_s on Errors

On using Equation (5) and assuming ν = 0.252, η = 0.05, and μ = 33 GPa, we obtain

$$\tau = 10^{0.75m_s - 1.5\log 2a - 0.77} \tag{21}$$

The allowable error in measuring m_s is 0.3, and hence the error of τ is

$$\tau + \Delta\tau = 10^{0.75(m_s+0.3) - 1.5\log 2a - 0.77} = 10^{0.75\times 0.3}\tau = 1.7\tau \tag{22}$$

The relative error $\Delta\tau/\tau$ can be as large as 70%.

2.2 Influence of a on Errors

There are two types of errors in determining the hypocentral radius r. The first error is caused by the use of the mean value of $\sin\theta$ on the focal sphere for evaluating the radiation pattern factor expressed as

$$t_{2\alpha} = r_h\left(\frac{1}{v_f} + \frac{\sin\theta}{v_p}\right) \tag{23}$$

By using the mean value of $\sin\theta$ on the focal sphere, Equation (23) becomes

$$t_{2\bar{\alpha}} = r_h\left(\frac{1}{v_f}+\frac{\pi}{4v_p}\right) \tag{24}$$

Here, we use v_f = 0.775v_s, and assume that v_s = 3.38 km/s (Wu et al., 1997) and v_p = 5.7 km/s (Giovambattista and Barba, 1997) within the crust. Also, we use $\bar{r}_h$ to denote the hypocentral radius evaluated using the mean value of $\sin\theta$ on the focal sphere, $(r_h)_{\max}$ to denote the radius evaluated by using the maximum value of $\sin\theta$ equal to 1, and $(r_h)_{\min}$ to denote the radius evaluated by using the maximum value of $\sin\theta$ equal to 0. The range of error in determining r_h can be calculated as

$$\frac{\left|\bar{r}_h-(r_h)_{\max}\right|}{(r_h)_{\max}} = \frac{\left|\dfrac{t_{2\alpha}}{\dfrac{1}{v_f}+\dfrac{\pi}{4v_p}}-\dfrac{t_{2\alpha}}{\dfrac{1}{v_f}+\dfrac{1}{v_p}}\right|}{\dfrac{t_{2\alpha}}{\dfrac{1}{v_f}+\dfrac{1}{v_p}}} \approx 0.073 \tag{25}$$

$$\frac{\left|\bar{r}_h-(r_h)_{\min}\right|}{(r_h)_{\min}} = \frac{\left|\dfrac{t_{2\alpha}}{\dfrac{1}{v_f}+\dfrac{\pi}{4v_p}}-\dfrac{t_{2\alpha}}{1/v_f}\right|}{\dfrac{t_{2\alpha}}{1/v_f}} \approx 0.265 \tag{26}$$

From Equations (25) and (26), it is found that the relative error of r_h varies from 7.3% to 26.5%. From Equations (21) and (22), it can be determined that the relative error in τ caused due to using the average value of $\sin\theta$ (in determining the hypocentral radius r_h) varies from 2.0% to 13.7%.

Another type of error is caused by the estimation of the corner frequency $f_{c\alpha}$. As shown in Equation (9), r_h can be estimated from $f_{c\alpha}$. We choose the window length T as 4 s and then the resolution becomes 0.25 Hz. For an earthquake whose magnitude is about M 3.0 and whose epicentral distance is 200 km, the corner frequency $f_{c\alpha}$ will be around 2.5 Hz. Thus, the relative error of $f_{c\alpha}$ may become 0.1. On substituting this value into Equation (8), it is found that the resulting relative error in a will be 1/(1+0.1) × 100% ≈ 9.1%. The consequent relative error in τ will be 2.7%. Based on the above discussion, it can be concluded that the error in evaluating the ambient stress τ is mainly caused by the error in estimating the earthquake magnitude m_s and that this error can be as much as 70%.

3. Summary

Based on the discussion in the last two sections, following conclusions are drawn:

1. The errors in determining the primary rupture directions are basically caused during the making of the generalized directional function plot. If the theoretical function curves are plotted versus θ at the interval of 15º, the maximum resultant error would be obtained as 15°.
2. The errors in evaluating the ambient stress τ are mainly caused by the error made in estimating the earthquake magnitude m_s. If the error caused in m_s is 0.3, the relative error caused in τ will be 70%.
3. The relative error in τ (between 2% and 14%) caused by using the mean value of $\sin\theta$ on the focal sphere may induce 7.3% to 26.5% error in the estimation of hypocentral radius r_h.

4. The use of $f_{c\alpha}$ to determine r_h generates a relative error of about 9.1%, which in turn leads to an error of 2% to 14% in determining the τ value.
5. The error due to digitization is about 1%, which may be considered acceptable.

CONCLUSIONS

This study has been based on four earthquake samples, which had the magnitudes of about 6.0 and which occured in the southern and eastern China since 1970. Six seismic wave parameters of these earthquakes have been analyzed and compared in order to investigate the abnormal phenomena taking place before the earthquakes, such as seismogenic zones and seismic belts. These parameters include the rupture characteristic L_0/L, primary rupture direction, the ambient shear stress τ, the temporal periodicity of waveform r, the Q value of P-waves, and the width of Fourier spectrum, w. Based on the analyses and discussions on the four earthquake samples, following remarks have been concluded:

1. The primary rupture directions of the earthquakes occuring on seismogenic zones are parallel to the nodal plane of the following main shock and those either are tangent to the zone or point outside the zone. However, during the normal periods, the primary rupture directions are disorganized.
2. The primary rupture directions of the earthquakes occuring on seismic belts are either close to the direction of the belt or conjugated to it (i.e., close to the direction of the primary rupture plane of the main shock), and are pointed in the same direction. For an earthquake that occurs during the normal periods, the primary rupture direction of the earthquake becomes different for a different area.
3. The strongest earthquake that occurs within 100 km from where the main shock occurs and within two years preceding the main shock can be defined as the foreshock. It has been found in the case of the earthquake samples considered that the ambient shear stress of the foreshock is much higher than that for the other earthquakes that occur in the same time period and that the foreshock shows a unilateral rupture.
4. As observed from the first three earthquake samples, there have been a few high values of ambient shear stress as well as acute changes in the shear stress during the small and medium earthquakes that occured in the year preceding the main shock and within 200 km from where the main shock occured, while during the other time periods, the shear stress stayed lower and varied smoothly. Shear stress is also correlated with the ranges of the magnitudes of small and medium earthquakes that occur before and after a main shock. Such a correlation has been observed from Tables 2, 4, 6, 8 with corresponding values of earthquakes magnitudes and larger values of shear stress have been obtained for those earthquakes with magnitudes ranging from 3.7 to 4.6 that mainly occurred before the main shock. Further, lower shear stress values have been obtained for the weaker earthquakes with magnitudes ranging from 2.5 to 3.5, most of which occurred after the main shock.
5. Except for the Heze earthquake, it has been found that during the period of several months to two years preceding the main shock, the temporal periodicity of waveform, r, changes violently, or at least more evidently, and several lower values may appear. In the normal periods, however, r is high and changes gently. Such a phenomenon has not been observed for the Heze earthquake due to the recorded data missing for the year before the earthquake (i.e., from November, 1982 to November, 1983).
6. The earthquakes that occur before the main shock are closer to a unilateral rupture (i.e., L_0/L is closer to 1.0) than those earthquakes that occur after the main shock, but this difference is not so distinct.
7. There is no distinct regularity in the variations for the Q values of P-waves and the width of Fourier spectrum before and after the main shock.
8. The quality factors (i.e., Q values) of a deep medium are higher than those of a shallow medium.

A limitation of this study is that the temporal variations have not been considered. In future, advanced statistical approaches would need to be developed in order to validate our conclusions regarding the relationship between the eventual changes in the trends and the occurrence of main shocks. In that case, a precursor would need to be associated with some of the changes occurring before a main shock. Further, the above eight remarks have been concluded based on the study of the analog records of only the earthquake examples considered with a limited number of shocks. Later on, it will be desirable to take the

help of advanced monitoring instruments and more complete and precise digital records, and to analyze more earthquake samples by following a similar approach to validate our conclusions. A systematic statistical analysis on the complete digital seismic records will help us to justify the conclusions drawn from this study better and to acquire more reliable correlations between the seismic parameters and seismic activities.

REFERENCES

1. Chen, P.-S., Gu, J.-C. and Li, W.-X. (1977). "Study of Earthquake's Rupture Process and Prediction Applying Rupture Mechanics", Chinese Journal of Geophysics, Vol. 20, No. 3, pp. 185–201 (in Chinese).
2. Chen, P.-S., Zhuo, Y.-R., Jin, Y., Wang, Z.-G., Huang, W.-Q., Li, W.-X. and Hu, R.-S. (1978). "Stress Field of Beijing, Tianjin, Tangshan, and Zhangjiakou Area before and after Tangshan Earthquake", Chinese Journal of Geophysics, Vol. 21, No. 1, pp. 24–58 (in Chinese).
3. Chen, Q.-F., Zheng, D.-L. and Che, S. (editors) (2002). "Earthquake Cases in China (1992–1994)", Seismological Press, Beijing, China (in Chinese).
4. Davies, J., Sykes, L., House, L. and Jacob, K. (1981). "Shumagin Seismic Gap, Alaska Peninsula: History of Great Earthquakes, Tectonic Setting, and Evidence for High Seismic Potential", Journal of Geophysical Research: Solid Earth, Vol. 86, No. B5, pp. 3821–3855.
5. Dorel, J. (1981). "Seismicity and Seismic Gap in the Lesser Antilles Arc and Earthquake Hazard in Guadeloupe", Geophysical Journal of the Royal Astronomical Society, Vol. 67, No. 3, pp. 679–695.
6. Feng, D.-Y. and Yu, X.-J. (1994). "Application of Seismic Wave's Dynamic Characteristics in Short Term Earthquake Prediction", Earthquake, Vol. 1, pp. 12–22 (in Chinese).
7. Gaudemer, Y., Tapponnier, P., Meyer, B., Peltzer, G., Guo, S.-M., Chen, Z.-T., Dai, H.-G. and Cifuentes, I. (1995). "Partitioning of Crustal Slip between Linked, Active Faults in the Eastern Qilian Shan, and Evidence for a Major Seismic Gap, the 'Tianzhu Gap', on the Western Haiyuan Fault, Gansu (China)", Geophysical Journal International, Vol. 120, No. 3, pp. 599–645.
8. Giovambattista, R.D. and Barba, S. (1997). "An Estimate of Hypocentre Location Accuracy in a Large Network: Possible Implications for Tectonic Studies in Italy", Geophysical Journal International, Vol. 129, No. 1, pp. 124–132.
9. Kagan, Y.Y. and Jackson, D.D. (1991). "Seismic Gap Hypothesis: Ten Years After", Journal of Geophysical Research: Solid Earth, Vol. 96, No. B13, pp. 21419–21431.
10. Kagan, Y.Y. and Jackson, D.D. (1995). "New Seismic Gap Hypothesis: Five Years After", Journal of Geophysical Research: Solid Earth, Vol. 100, No. B3, pp. 3943–3959.
11. Kostoglodov, V., Singh, S.K., Santiago, J.A., Franco, S.I., Larson, K.M., Lowry, A.R. and Bilham, R. (2003). "A Large Silent Earthquake in the Guerrero Seismic Gap, Mexico", Geophysical Research Letters, Vol. 30, No. 15, Paper 1807.
12. Lahr, J.C. and Plafker, G. (1980). "Holocene Pacific-North American Plate Interaction in Southern Alaska: Implications for the Yakataga Seismic Gap", Geology, Vol. 8, No. 10, pp. 483–486.
13. Lidaka, T., Kato, A., Kurashimo, E., Iwasaki, T., Hirata, N., Katao, H., Hirose, I. and Miyamachi, H. (2009). "Fine Structure of P-Wave Velocity Distribution along the Atotsugawa Fault, Central Japan", Tectonophysics, Vol. 472, No. 1-4, pp. 95–104.
14. Liu, W.-L., Wu, P.-Z. and Chen, Y.-W. (1996). "Determination of Earthquake's Rupture Characteristics Using Directional Function", Earthquake Research in China, Vol. 12, No. 1, pp. 93–99 (in Chinese).
15. Liu, Z.-K., Wang, W., Zhang, R., Yu, N.-H., Zhang, T.-Z. and Pan, J.-Y. (2001). "A Seismogram Digitization and Database Management System", Acta Seismologica Sinica, Vol. 14, No. 3, pp. 333–341 (in Chinese).
16. Peacock, S., Crampin, S., Booth, D.C. and Fletcher, J.B. (1988). "Shear Wave Splitting in the Anza Seismic Gap, Southern California: Temporal Variations as Possible Precursors", Journal of Geophysical Research: Atmospheres, Vol. 93, No. B4, pp. 3339–3356.

17. Venkataraman, A. (2002). “Investigating the Mechanics of Earthquakes Using Macroscopic Seismic Parameters”, Ph.D. Thesis, Division of Geological and Planetary Sciences, California Institute of Technology, Pasadena, U.S.A.
18. Wu, F.T., Levshin, A.L. and Kozhevnikov, V.M. (1997). “Rayleigh Wave Group Velocity Tomography of Siberia, China and the Vicinity”, Pure and Applied Geophysics, Vol. 149, No. 3, pp. 447–473.
19. Zhang, Z.-C., Luo, L.-G., Li, H.-H., Chen, L.-D. and Li, X.-H. (editors) (1990a). “Earthquake Cases in China (1976–1980)”, Seismological Press, Beijing, China (in Chinese).
20. Zhang, Z.-C., Luo, L.-G., Li, H.-H., Chen, L.-D. and Li, X.-H. (editors) (1990b). “Earthquake Cases in China (1981–1985)”, Seismological Press, Beijing, China (in Chinese).